

# Microscopic derivation of $\pi - N(\Delta)$ scattering lengths

P. Bicudo,\* M. Faria, G. M. Marques,<sup>†</sup> and J. E. Ribeiro<sup>‡</sup>

*Centro de Física das interacções Fundamentais (CFIF),*

*Departamento de Física, Instituto Superior Técnico,*

*Av. Rovisco Pais, 1049-001 Lisboa, Portugal*

## Abstract

A general expression for the  $\pi - N$  and  $\pi - \Delta$  scattering lengths is derived in the framework of a microscopic calculation. A comparison with  $\pi - \pi$  scattering is also provided. For  $\pi - \pi$  is shown that the Ward identities ensure the cancellation of all scalar microscopic interactions for us to have the Weinberg results for the scattering lengths. The point-like limit is used as an expeditious way to calculate the  $\pi - \pi$  scattering lengths. This limit is also used to evaluate  $\pi - N$  and  $\pi - \Delta$  scattering lengths. The scalar microscopic contributions for  $\pi - N$  and  $\pi - \Delta$  scattering are shown to vanish trivially in this limit. Numerical values for  $\pi - N$  and  $\pi - \Delta$  scattering lengths are given. Going outside the point-like limit is discussed both for  $\pi - \pi$  and  $\pi - N(\Delta)$

---

\*Electronic address: bicudo@ist.utl.pt

<sup>†</sup>Electronic address: gmarques@cfif.ist.utl.pt

<sup>‡</sup>Electronic address: emilio@atlas.ist.utl.pt

## I. INTRODUCTION

In the last decade a global picture for low energy hadronic physics has slowly emerged. Although the theory of hadronic reactions, which one expects to be a consequence of QCD, remains as challenging as ever, it possesses a natural symmetry (chiral symmetry) which acts, so to speak, as a filter for the still largely unknown low energy details of strong interactions. Indeed it is remarkable that although intermediate theoretical concepts like gluon propagators, quark effective masses and so on, might vary (in fact they are not gauge invariant and hence they are not physical observables), chiral symmetry contrives for the final physical results, e.g. hadronic masses and scattering lengths, to be largely insensitive to the above mentioned theoretical uncertainties. The pion mass furnishes the ultimate example. For massless quarks, the pion mass is bound to be zero, regardless of the form of the effective quark interaction *provided* it supports the mechanism of spontaneous breakdown of chiral symmetry ( $S\chi SB$ ).

$\pi - \pi$  elastic scattering [1] provides another example of this insensitivity to the form of the quark microscopic interaction. The incorporation of chiral symmetry in quark models has, in the history of hadronic physics, a long standing, starting with the attempts at restoring chiral symmetry to the MIT bag model [2, 3, 4, 5]. Those models can be considered as realizations of a more general class of microscopic models, known as extended Nambu–Jona–Lasinio models (eNJL), which in turn could be formally deduced from QCD through cumulant expansion [6] if we were to know all the gluon correlators. However, for practical applications, the set of all gluon correlators gets reduced to the Gaussian approximation (two gluon correlators). It simply turns out that chiral symmetry alleviates us from the burden of knowing in detail even this correlator. The initial studies within eNJL models were aimed at studying the interplay between confinement and dynamical chiral symmetry breaking ( $D\chi SB$ ), and concentrated on critical couplings [7] for  $D\chi SB$  and light meson spectroscopy [8]. Those NJL like models have been extended to study the pion beyond BCS level and meson resonant decays in the context of a generalized resonating group method [9, 10]. It is also important to observe that these calculations can be redone in the Euclidean spacetime [11]. The paper is organized as follows: in Chapter II we briefly introduce the Hamiltonian description of  $D\chi SB$ . From there we will proceed in a systematic way in terms of external hadron sources. We start in Chapter III by having no external sources and show the corresponding class of Feynman diagrams (vacuum bubbles) to lead to the mass gap equation as a minimization requirement of the vacuum energy density. Next, in Chapter IV, we consider the infinite set of Feynman diagrams which can be obtained in the presence of two external hadronic sources and show the infinite ladder sum of such diagrams to lead to the Salpeter amplitude for the corresponding hadron. The pion is shown to correspond to the Goldstone boson of chiral symmetry for massless quarks. Finally in Chapter V we consider the case of 4 external pion sources and, using the same formalism, re-derive [12] the  $\pi - \pi$  scattering lengths and then show them to coincide with the Weinberg results. Chapter VI deals with the issue of going beyond the RGM approximation. Chapter VII is devoted to the discussion of  $\pi - N(\Delta)$  scattering. We close with Chapter VIII. Intermediate results are provided in three appendices.

## II. THE HAMILTONIAN DESCRIPTION OF $D\chi SB$

To be more specific, the eNJL class of models correspond to the Gaussian approximation of QCD in the cumulant expansion in terms of gluon correlators,

$$H = \int d^3x q^\dagger(x)(-i\alpha \cdot \nabla + m\beta)q(x) - \frac{i}{2} \int d^3x \int d^3y \bar{q}(x)\gamma^\mu T^a q(x) \bar{q}(y)\gamma^\nu T^b q(y) \langle\langle gA_\mu^a(x)gA_\nu^b(y) \rangle\rangle, \quad (2.1)$$

where we have introduced the traditional notation  $\beta = \gamma^0$  and  $\alpha^i = \gamma^0\gamma^i$ . The Gaussian correlator  $\langle\langle gA_\mu^a(x)gA_\nu^b(y) \rangle\rangle$  turns out to be identical to the vacuum expectation  $\langle gA_\mu^a(x)gA_\nu^b(y) \rangle$ . In Eq.(2.1) the  $T^a$  stand for the Gell-Mann generators  $\lambda^a/2$ .

Although these correlators, taken as functions  $\mathcal{K} = T^a K_{ab}^{\mu\nu}(x, y) T^b$  are gauge dependent quantities and in general they do depend on the chosen gauge, it happens that, at least in the instantaneous limit  $\mathcal{K} = T^a k_{ab}^{\mu\nu}(\mathbf{x}, \mathbf{y}) T^b$ , the low energy hadronic scattering lengths turn out to be *independent* of the chosen  $k(\mathbf{x}, \mathbf{y})$ . This we will show by re-deriving the  $\pi - \pi$  Weinberg results for the class of models embodied by Eq.(2.1). This will act not only as an introduction to the more elaborated  $\pi - N(\Delta)$  but also as a validation criterium for the application of these class of models to generic low energy hadronic scattering processes.

FIG. 1: Mass gap equation as a variational minimum of the vacuum energy in  $\varphi(k'')$ . The symbols  $\{+,-\}$  stand for the quark propagator projection operators  $\{\Lambda^+, \Lambda^-\}$ , which are given by,  $\Lambda^\pm(\mathbf{k}) = (1 \pm \sin(\varphi)\beta \pm \cos(\varphi) \boldsymbol{\alpha} \cdot \hat{\mathbf{k}})/2$ .

### III. NO EXTERNAL SOURCES: THE MASS GAP EQUATION

The simplest set of diagrams we can consider are provided by the vacuum diagrams depicted in Fig. 1. These diagrams give the vacuum energy  $\int d^3x \mathcal{E}$ . Then, to derive the mass gap equation it is enough to find the variational minimum of the vacuum energy density  $\mathcal{E}$  in terms of  $\varphi$ . We get,

$$\int d^3x \delta \left[ 3 \int \frac{d^3k}{(2\pi)^3} \text{Tr} \left( (\boldsymbol{\alpha} \cdot \mathbf{k} + m_q \beta) \Lambda^-(\mathbf{k}) \right) + \int \frac{d^3k}{(2\pi)^3} \int \frac{d^3k'}{(2\pi)^3} V_{ab}^{\mu\nu}(\mathbf{k} - \mathbf{k}') \text{Tr} \left( \Lambda^-(\mathbf{k}') T^b \gamma_\nu \Lambda^+(\mathbf{k}) T^a \gamma_\mu \right) \right] = 0, \quad (3.1)$$

where  $V_{ab}^{\mu\nu}(\mathbf{k} - \mathbf{k}')$  corresponds to the Fourier transform of  $k_{ab}^{\mu\nu}(\mathbf{x}, \mathbf{y})$ .  $\Delta^\pm$  denote the Feynman projectors – see appendix A. Physically, the mechanism of spontaneous breaking of chiral symmetry can be understood as a self-consistent choice of the fermion Fock space appropriated to the quark kernel  $\mathcal{K}$  in use. In principle, the set of all Fock spaces consistent with the Pauli principle is infinite and can be mapped to an infinite set of given functions of space-time coordinates, the so-called chiral angles  $\varphi$ . Any such Fock space can be obtained from the trivial one by a Valatin-Bogoliubov transformation with parameter  $\varphi$ . The actual form of such functions is determined by solving the mass gap equation. For examples of mass gap equations and solutions, see Ref. [9] for the harmonic confining kernel  $V(x) = K_0^3 x^2$  and Refs. [13, 14] for the linear case  $V(x) = \sigma x$  with  $\sigma = K_0^2$ . Finally, the Dirac field  $\Psi$  can be thought as an inner product between the spinors Hilbert space and the Fock space, with the property of being *invariant* under Valatin-Bogoliubov rotations so that a rotation in the Fock space should engender a counter rotation of the spinors by the same amount  $\varphi$ ,

$$u_s(\mathbf{p}) = \left[ \sqrt{\frac{1 + \sin \varphi}{2}} + \sqrt{\frac{1 - \sin \varphi}{2}} \hat{\mathbf{p}} \cdot \boldsymbol{\alpha} \right] u_s(\mathbf{0}); \quad v_s(\mathbf{p}) = \left[ \sqrt{\frac{1 + \sin \varphi}{2}} - \sqrt{\frac{1 - \sin \varphi}{2}} \hat{\mathbf{p}} \cdot \boldsymbol{\alpha} \right] v_s(\mathbf{0}). \quad (3.2)$$

For zero momentum we always have, regardless of the strength of the microscopic quark-quark interaction,  $\varphi(0) = \pi/2$ . It happens that the mass gap equation (of which  $\varphi(k)$  is the solution) possesses, for massless particles, only one scale, the microscopic quark kernel strength  $K_0$ . Therefore we can plot  $\varphi(k)$ , for all  $K_0$ , in terms of a dimensionless variable  $k_a = k/K_0$ , so that there is only one  $\varphi(k_a)$  per class of quark kernel: one for linear confining kernels, another for the harmonic kernel and so on. Naturally we can, for a given  $K_0$  measured for instance in MeV, replot  $\varphi(k_a)$  as  $\varphi(k)$  with now  $k$  being measured in MeV. Thus, for different confining scales  $K_0$  we generate different  $\varphi(k)$  which are the solutions of the mass gap for that particular strength  $K_0$ . Again  $\varphi(k_a = 0) = \pi/2$ . Then it is not difficult to see that when  $K_0 \rightarrow \infty$  we have  $k_a = 0$  and  $\varphi(k) = \pi/2$  for all finite  $k$ . Alternatively this can be seen by plotting  $\varphi(k)$  for various  $K_0$  and seeing this function approaching  $\pi/2$  for larger and larger  $K_0$ . We call this limit, the point-like limit because in coordinate space it corresponds to point-like bound states.

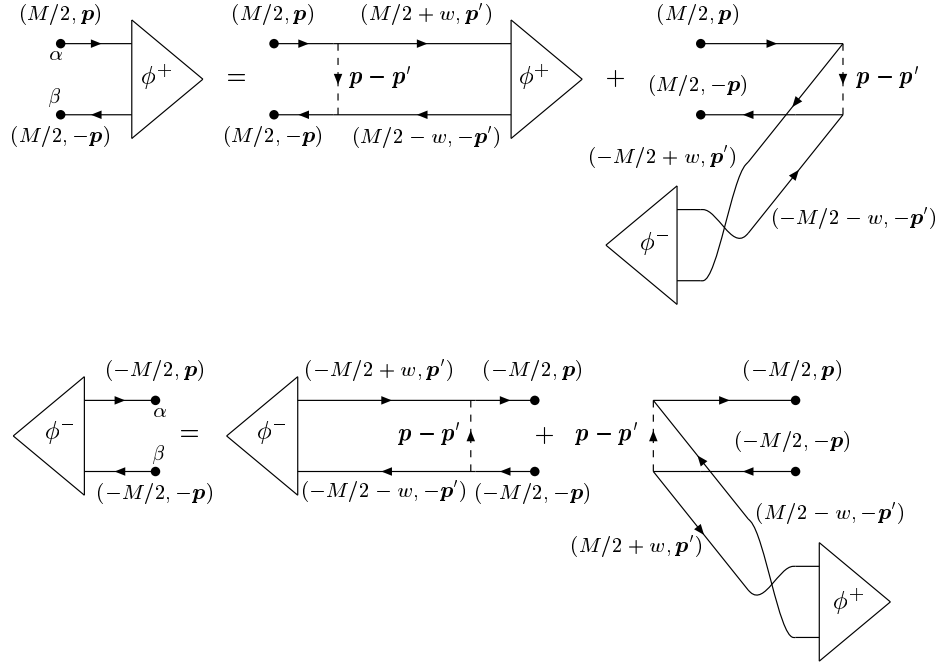


FIG. 2: Pion Salpeter Equations as a set of two coupled, self-referring Feynman diagrams. The dots stand for the amputation of the Feynman propagators. Because we have an instantaneous interaction, the integration in the energy loop  $\omega$  will select from the full quark propagators only one of the two components – either quark or antiquark. – either  $\Lambda^+$  or  $\Lambda^-$  – as they are indicated by the symbols + or – respectively. The other combinations yield zero.

Another remarkable feature of the mechanism of  $D\chi SB$  is the appearance of a pion Goldstone boson. The simplest way to understand this is to notice that the axial charge  $Q_5 = \int \bar{\Psi} \gamma_0 \gamma_5 \Psi$  contains an anomalous Bogoliubov term which can no longer be set to zero, *once* we have chosen to set (for the sake of vacuum time translation stability) the anomalous Bogoliubov term present in the Hamiltonian to zero. It can be shown that setting the anomalous term in the Hamiltonian to zero is *tantamount* to derive the mass gap equation. Using Eq.(3.2) we obtain,

$$\int d^3x \bar{\psi}(\mathbf{x}) \gamma_0 \gamma_5 \psi(\mathbf{x}) = \int \frac{d^3p}{(2\pi)^3} \left[ \cos(\varphi(p)) \left( \hat{\mathbf{p}} \cdot \boldsymbol{\sigma}_{ss'} b_s^\dagger(\mathbf{p}) b_{s'}(\mathbf{p}) + \hat{\mathbf{p}} \cdot \boldsymbol{\sigma}_{ss'}^* d_s(-\mathbf{p}) d_{s'}^\dagger(-\mathbf{p}) \right) - \sin(\varphi(p)) \left( i\sigma_{ss'}^2 b_s^\dagger(\mathbf{p}) d_{s'}^\dagger(-\mathbf{p}) - i\sigma_{ss'}^2 d_s(-\mathbf{p}) b_{s'}(\mathbf{p}) \right) \right]. \quad (3.3)$$

Then the  $Q_5$  anomalous term, proportional to  $\sin(\varphi(p))$ , creates a pion excitation from the vacuum. This pion has zero mass because  $Q_5$  commutes with  $H$ . The Salpeter wave functions of the *real* pion are determined from the RPA equation,  $[H, Q_5] = m_\pi Q_5$  or, equivalently, by solving the corresponding Salpeter equation – see Refs. [10, 13, 14]. The Salpeter amplitude  $\sin(\varphi(p))$  coincides with the above simple derivation.

## IV. ADDING TWO EXTERNAL SOURCES

### A. The $\pi \rho N \Delta$ Bound States

The Salpeter equation for a meson is depicted in Fig. 2 and translates to:

$$\begin{aligned} \phi_{\alpha\beta}^+ &= \int \frac{d^4 p'}{(2\pi)^4} \frac{m}{E_q(\mathbf{p}')} \Gamma_{\alpha\mu}^{--} \frac{-i}{-(M/2 - w) - E_q(-\mathbf{p}') + i\epsilon} \phi_{\mu\nu}^+(M, \mathbf{p}') \frac{i}{(M/2 + w) - E_q(\mathbf{p}') + i\epsilon} \Gamma_{\nu\beta}^{++}(-i\mathcal{K}(\mathbf{p} - \mathbf{p}')) + \\ &+ \int \frac{d^4 p'}{(2\pi)^4} \frac{m}{E_q(\mathbf{p}')} \Gamma_{\alpha\mu}^{-+} \frac{i}{(-M/2 - w) - E_q(-\mathbf{p}') + i\epsilon} \phi_{\mu\nu}^+(M, \mathbf{p}') \frac{-i}{(-M/2 + w) - E_q(\mathbf{p}') + i\epsilon} \Gamma_{\nu\beta}^{+-}(-i\mathcal{K}(\mathbf{p} - \mathbf{p}')) , \\ \phi_{\alpha\beta}^- &= \int \frac{d^4 p'}{(2\pi)^4} \frac{m}{E_q(\mathbf{p}')} \Gamma_{\alpha\mu}^{++} \frac{i}{(-M/2 + w) - E_q(\mathbf{p}') + i\epsilon} \phi_{\mu\nu}^-(M, \mathbf{p}') \frac{-i}{(-M/2 - w) - E_q(-\mathbf{p}') + i\epsilon} \Gamma_{\nu\beta}^{--}(-i\mathcal{K}(\mathbf{p} - \mathbf{p}')) + \\ &+ \int \frac{d^4 p'}{(2\pi)^4} \frac{m}{E_q(\mathbf{p}')} \Gamma_{\alpha\mu}^{-+} \frac{-i}{-(M/2 - w) - E_q(-\mathbf{p}') + i\epsilon} \phi_{\mu\nu}^-(M, \mathbf{p}') \frac{i}{-(M/2 + w) - E_q(\mathbf{p}') + i\epsilon} \Gamma_{\nu\beta}^{+-}(-i\mathcal{K}(\mathbf{p} - \mathbf{p}')) . \end{aligned} \quad (4.1)$$

In this equation we have only two kinds of microscopic quark-quark interactions –Fig.3(a) and 3(d)– out of the possible four. This is easily understood by noticing that the result of an energy loop integral with just two quark propagators or two antiquark propagators vanishes, since their poles are on the same side of the axis. Hence, the omission of these interactions in the middle of the ladders is clear. For the pion case we have,

$$V_\pi^{++}(\mathbf{p}, \mathbf{q}) = \frac{4}{3} \text{Tr}\{\Sigma^\pi \cdot \Gamma_{p,q}^{--} \cdot \Sigma^\pi \cdot \Gamma_{q,p}^{++}\} V(\mathbf{p} - \mathbf{q}) = -\frac{2}{3} \text{Tr}\{\Gamma_{p,q}^{++} \Gamma_{q,p}^{++}\} V(\mathbf{p} - \mathbf{q}), \quad (4.2)$$

$$V_\pi^{+-}(\mathbf{p}, \mathbf{q}) = \frac{4}{3} \text{Tr}\{\Sigma^\pi \cdot \Gamma_{p,q}^{-+} \cdot \Sigma^\pi \cdot \Gamma_{q,p}^{-+}\} V(\mathbf{p} - \mathbf{q}) = \frac{2}{3} \text{Tr}\{\Gamma_{p,q}^{+-} \Gamma_{q,p}^{+-}\} V(\mathbf{p} - \mathbf{q}). \quad (4.3)$$

where,

$$\begin{aligned} \Gamma_{p,q}^{++} &= u_p^\dagger \beta \Gamma u_q, \quad \Gamma_{p,q}^{+-} = u_p^\dagger \beta \Gamma v_q, \\ \Gamma_{p,q}^{-+} &= v_p^\dagger \beta \Gamma u_q, \quad \Gamma_{p,q}^{--} = -v_p^\dagger \beta \Gamma v_q. \end{aligned} \quad (4.4)$$

$\Sigma^\pi$  stands for the pion spin wave function that is defined in Appendix B 2 along with spin wave functions of other relevant hadrons.  $V(\mathbf{p} - \mathbf{q})$  represents the Fourier transform of a generic quark kernel which we do not have to know. To derive Eqs.(4.2) and (4.3) we have followed reference [9] where the Bogoliubov rotated spinors of Eq.(3.2), carrying the information on the chiral angle  $\varphi$ , have been associated with the usual  $\Gamma$  vertex, therefore yielding the four effective quark-kernel vertices  $\Gamma^{\pm\pm}$  of Eq.(4.4), rather than having them, as it is usual in diagrammatic techniques, inside the Feynman propagators  $G_{\text{Feyn}}$ . For the Dirac matrices  $\Gamma = \beta$  or  $\Gamma = \alpha$ , the following properties hold,

$$\Gamma^{--} = (i\sigma^2)\Gamma^{++}(i\sigma^2), \quad \Gamma^{-+} = (i\sigma^2)\Gamma^{+-}(i\sigma^2). \quad (4.5)$$

Using equations (4.2), (4.4) and (4.5) we are able to draw the Goldstone diagrams of Fig.4 – representing the Salpeter equation for the pion. A similar expression can be written for the  $\rho$ ,

$$V_\rho^{++}(\mathbf{p}, \mathbf{q}) = \frac{4}{3} \text{Tr}\{\Sigma_s^\rho \cdot \Gamma^{--} \cdot \Sigma_{s'}^{\rho\dagger} \cdot \Gamma^{++}\} V(\mathbf{p} - \mathbf{q}) = -\frac{2}{3} \text{Tr}\{\sigma^i \Gamma^{++} \sigma^j \Gamma^{++}\} v_{s'}^j v_s^i V(\mathbf{p} - \mathbf{q}). \quad (4.6)$$

The potential  $V_\rho^{+-}(\mathbf{p}, \mathbf{q})$  is proportional to  $V_\pi^{+-}(\mathbf{p}, \mathbf{q})$ . In this formalism  $G_{\text{Feyn}}$  turns out to be very simple,

$$G_{\text{Feyn}} = \frac{i}{w - E(\mathbf{p})}. \quad (4.7)$$

We find this formalism, also used in [9], more amenable to a physical visualization in terms of Goldstone diagrams. Of course the two formalisms are absolutely identical, the translation between these two formalisms being provided by the pole decomposition of the Dirac operator,

$$\begin{aligned} S &= \frac{i}{A(k) \cdot \mathbf{k} + B(k)} = \frac{i}{k^0 \beta - E(k) \left\{ \sin[\varphi(k)] + \cos[\varphi(k)] \hat{\mathbf{k}} \cdot \boldsymbol{\gamma} \right\} + i\epsilon} \\ &= \sum_s \frac{u_s(k) i u_s(k)^\dagger \beta}{k^0 - E(\mathbf{k}) + i\epsilon} - \frac{v_s(k) i v_s(k)^\dagger \beta}{-k^0 - E(\mathbf{k}) + i\epsilon}, \end{aligned} \quad (4.8)$$

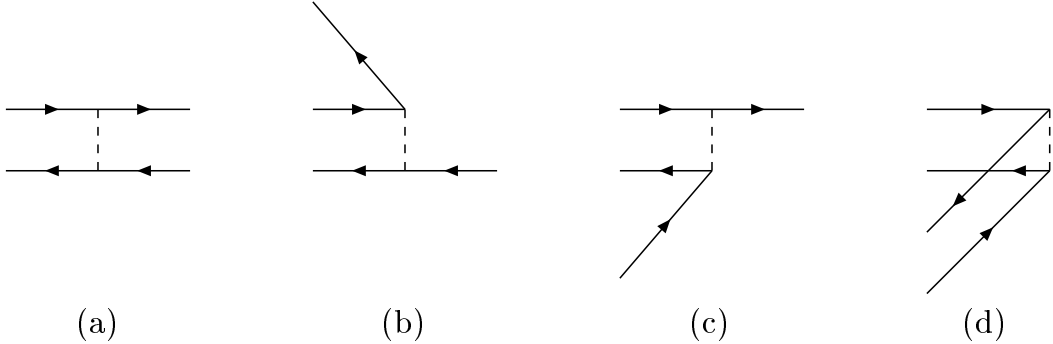


FIG. 3: The four types of interactions that appear from the decomposition of the propagators.

where  $u$  and  $v$  are the Dirac spinors of Eq.(3.2) and  $E(\mathbf{k})$  is the energy of the quark and the antiquark. From Eq.(4.1) it is clear that we can trivially integrate out the loop energy  $w$  yielding a global propagator  $G^0$  for the pion

$$G^0(M, \mathbf{p}') = i/(M - E_q(-\mathbf{p}') - E_q(\mathbf{p}')) . \quad (4.9)$$

Finally we redefine new Salpeter amplitudes as

$$G^0(M, \mathbf{p}') \phi_{\alpha\beta}^{\pm}(M, \mathbf{p}) \rightarrow \phi_{\alpha\beta}^{\pm}(M, \mathbf{p}) , \quad (4.10)$$

to obtain a Schrödinger-like [10] equation for the pion (the same could have been done for any meson),

$$H \begin{bmatrix} \phi^+(\mathbf{q}) \\ \phi^-(\mathbf{q}) \end{bmatrix} = \begin{bmatrix} 2T + V^{++}(\mathbf{p}, \mathbf{q}) & V^{+-}(\mathbf{p}, \mathbf{q}) \\ V^{-+}(\mathbf{p}, \mathbf{q}) & 2T + V^{--}(\mathbf{p}, \mathbf{q}) \end{bmatrix} \begin{bmatrix} \phi^+(\mathbf{q}) \\ \phi^-(\mathbf{q}) \end{bmatrix} = m \sigma^3 \begin{bmatrix} \phi^+(\mathbf{p}) \\ \phi^-(\mathbf{p}) \end{bmatrix} \quad (4.11)$$

An integration over  $\mathbf{q}$  is implied.  $T$  represents the kinetic operator.  $\{\phi^+, \phi^-\}$  are the RPA quark-antiquark Salpeter amplitudes for positive, negative energies. The pion occupies a singular position, insofar it is the only bound state where these two amplitudes have similar magnitudes. In all other cases  $|\phi^-|$  is smaller than  $|\phi^+|$ . For large current quark masses  $\phi^-$  goes to zero and we recover the usual Schrödinger picture. In the case of the pion and for massless current quarks these two amplitudes are identical, we have a Goldstone boson, and the corresponding Salpeter amplitude ceases to be normalizable. This extra amplitude  $\phi^-$  must enter in all reactions involving the pion and, as we will see, this extra degree of freedom is all what it takes to obtain the low energy pion mediated interactions.

The solutions (eigenvectors) of the Bethe-Salpeter equation (4.11) are normalized as follows,

$$[\phi^+(\mathbf{k}) \ \phi^-(\mathbf{k})] \sigma^3 \begin{bmatrix} \phi^+(\mathbf{k}) \\ \phi^-(\mathbf{k}) \end{bmatrix} = \int \frac{d^3 k}{(2\pi)^3} (\phi^+(\mathbf{k})^2 - \phi^-(\mathbf{k})^2) = 1. \quad (4.12)$$

The Salpeter pion wave functions are

$$\phi^{\pm}(k) = \frac{\sin[\varphi(k)]}{a} \pm a \Delta(k) \quad \text{with} \quad a = \sqrt{\frac{2m_\pi}{3}} f_\pi , \quad (4.13)$$

$f_\pi$  is the well known pion decay constant.

When we exchange  $\phi^+ \leftrightarrow \phi^-$ , we have that  $m_\pi \leftrightarrow -m_\pi$ . Then when  $\phi^+ = \phi^-$  we have  $m_\pi = 0$  (chiral limit). This is the Goldstone pion. In this particular case  $\phi^+(k) = \phi^-(k) \propto \sin(\varphi(k))/a$  and  $\pi$  ceases to be normalized.  $\sin(\varphi(k))$  determines the extent of dynamical chiral symmetry breaking and  $\Delta(k)$  is related to normalization of the wave function,

$$[\phi^+(\mathbf{k}) \ \phi^-(\mathbf{k})] \sigma^3 \begin{bmatrix} \phi^+(\mathbf{k}) \\ \phi^-(\mathbf{k}) \end{bmatrix} = \int \frac{d^3 k}{(2\pi)^3} 4 \sin(\varphi(\mathbf{k})) \Delta(\mathbf{k}) = 1. \quad (4.14)$$

The quark condensate  $\langle \bar{\psi} \psi \rangle$  is given by,

$$\langle \bar{\psi} \psi \rangle = - \int \frac{d^3 k}{(2\pi)^3} 6 \sin(\varphi(\mathbf{k})). \quad (4.15)$$

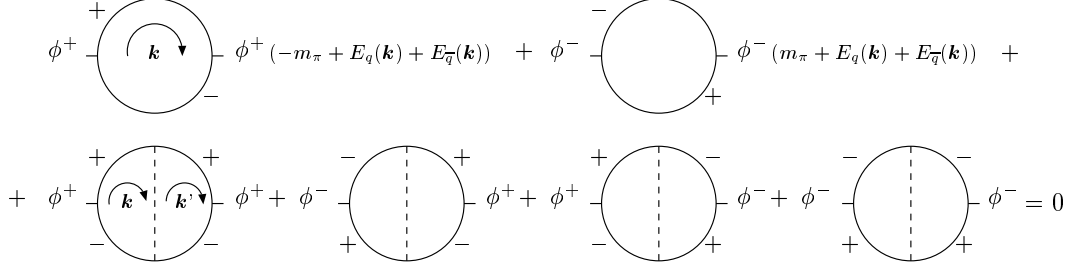


FIG. 4: Salpeter equation for  $\pi$ . Notice that  $\phi^\pm$  consistent with the normalization condition of Eq.(4.14) should contain the cluster propagators obtained after integration in energy of the quark propagators. This is the reason of the propagator cuts displayed in the figure. The factor  $\pm m_\pi + E_q + E_{\bar{q}}$  appearing in the normalization diagrams stem precisely from the fact that we need two such cluster propagators to go with two  $\phi$ 's and we only get one per integration loop so that we have to multiply and divide these diagrams by the missing cluster propagator.



FIG. 5: Baryon Salpeter equation.

The Salpeter equation for mesons, being self-referred, as it is clear from the figure 2, will yield an infinite set of ladder diagrams. Conversely we can re-sum such ladders to obtain [10]

$$\sum \text{ladder} = \sum_{\alpha, \beta} \phi^\alpha \frac{1}{E - M + i\epsilon} \phi^\beta. \quad (4.16)$$

In the case of the pion  $\phi^\alpha$  stands for one of the Salpeter amplitudes  $\phi^\pm$ . Hence in the Hilbert space of pion Salpeter amplitudes, the Hamiltonian,

$$H_\pi = \begin{bmatrix} H^{++} & H^{+-} \\ H^{-+} & H^{--} \end{bmatrix}_\pi = \begin{bmatrix} 2T + V_\pi^{++} & V_\pi^{+-} \\ V_\pi^{-+} & 2T + V_\pi^{--} \end{bmatrix} \quad (4.17)$$

can be written as,

$$H_\pi = \sigma_3 \begin{bmatrix} \phi^+ \\ \phi^- \end{bmatrix} m_\pi [\phi^+, \phi^-] \sigma_3 + \sigma_3 \begin{bmatrix} \phi^- \\ \phi^+ \end{bmatrix} m_\pi [\phi^-, \phi^+] \sigma_3 \quad (4.18)$$

with,

$$H_\pi \begin{bmatrix} \phi^+ \\ \phi^- \end{bmatrix} = m_\pi \sigma_3 \begin{bmatrix} \phi^+ \\ \phi^- \end{bmatrix}; H_\pi \begin{bmatrix} \phi^- \\ \phi^+ \end{bmatrix} = -m_\pi \sigma_3 \begin{bmatrix} \phi^- \\ \phi^+ \end{bmatrix}. \quad (4.19)$$

In the chiral limit Eq.(4.19) can be simply recast as,

$$\int \sin \varphi (H_\pi^{++} + H_\pi^{+-}) \sin \varphi = 0. \quad (4.20)$$

## B. $\mathbf{N}$ and $\Delta$ Schrödinger equations

The baryons also possess a Bethe-Salpeter equation. Normally there will be a positive energy and a negative energy component as well as mixed components (like a two quarks and an antiquark), but as the baryons are quite massive, the negative energy components can be neglected. Thus the Bethe-Salpeter equation becomes (see Fig. 5),

$$\begin{aligned}
\Psi_{\alpha\beta\delta} = - \int \frac{d^4k}{(2\pi)^4} \frac{m}{E_q(\mathbf{k})} \left( \frac{\Gamma_{\alpha\mu}^{++} \Psi_{\mu\nu\delta}(\mathbf{p}_1 - \mathbf{k}, \mathbf{p}_2 + \mathbf{k}, \mathbf{p}_3) \Gamma_{\nu\beta}^{++}(-i\mathcal{K}(\mathbf{k}))}{(E_1 - w - E_q(\mathbf{p}_1 - \mathbf{k}) + i\epsilon) (E_2 + w - E_q(\mathbf{p}_2 + \mathbf{k}) + i\epsilon)} + \right. \\
+ \frac{\Gamma_{\alpha\mu}^{++} \Psi_{\mu\beta\nu}(\mathbf{p}_1 - \mathbf{k}, \mathbf{p}_2, \mathbf{p}_3 + \mathbf{k}) \Gamma_{\nu\delta}^{++}(-i\mathcal{K}(\mathbf{k}))}{(E_1 - w - E_q(\mathbf{p}_1 - \mathbf{k}) + i\epsilon) (E_3 + w - E_q(\mathbf{p}_3 + \mathbf{k}) + i\epsilon)} + \\
\left. + \frac{\Gamma_{\beta\mu}^{++} \Psi_{\alpha\mu\nu}(\mathbf{p}_1, \mathbf{p}_2 - \mathbf{k}, \mathbf{p}_3 + \mathbf{k}) \Gamma_{\nu\delta}^{++}(-i\mathcal{K}(\mathbf{k}))}{(E_2 - w - E_q(\mathbf{p}_1 - \mathbf{k}) + i\epsilon) (E_3 + w - E_q(\mathbf{p}_3 + \mathbf{k}) + i\epsilon)} \right). \tag{4.21}
\end{aligned}$$

After computing the energy loops the equation becomes a Shrödinger-like (integral) equation:

$$H_{N,\Delta}\Psi = M_{N,\Delta}\Psi \tag{4.22}$$

where we have simply

$$H_{N,\Delta} = H_{N,\Delta}^{++} = T_1 + T_2 + T_3 + V_{N,\Delta}^{12} + V_{N,\Delta}^{13} + V_{N,\Delta}^{23} = 3T + V_{N,\Delta}^{++}. \tag{4.23}$$

In the same way as we did for  $\pi$  and  $\rho$  we compute the potential terms:

$$\begin{aligned}
V_{N^F}^{++}(\mathbf{p}, \mathbf{q}) &= 3\frac{2}{3} \text{Tr}\{\Sigma_s^{N^F} \cdot \Gamma_{p-k, q-k}^{++} \cdot \Sigma_{s'}^{N^F\dagger} \cdot \Gamma_{p,q}^{++}\} V(\mathbf{k}) = \\
&= -3\frac{1}{3} \text{Tr}\{\Gamma_{q-k, p-k}^{++} \Gamma_{p,q}^{++}\} \delta_{ss'} V(\mathbf{k}) = \frac{3}{2} V_\pi^{++} \delta_{ss'}, \tag{4.24}
\end{aligned}$$

$$\begin{aligned}
V_{N^D}^{++}(\mathbf{p}, \mathbf{q}) &= 3\frac{2}{3} \text{Tr}\{\Sigma_s^{N^D} \cdot \Gamma_{p-k, q-k}^{++} \cdot \Sigma_{s'}^{N^D\dagger} \cdot \Gamma_{p,q}^{++}\} V(\mathbf{k}) = \\
&= -3\frac{1}{3} \text{Tr}\{\sigma^i \Gamma_{q-k, p-k}^{++} \sigma^j \Gamma_{p,q}^{++}\} \sigma_{sc}^i \sigma_{cs'}^j V(\mathbf{k}) = \frac{3}{2} V_\rho^{++} \delta_{ss'}, \tag{4.25}
\end{aligned}$$

$$\begin{aligned}
V_\Delta^{++}(\mathbf{p}, \mathbf{q}) &= 3\frac{2}{3} \text{Tr}\{\Sigma_s^\Delta \cdot \Gamma_{p-k, q-k}^{++} \cdot \Sigma_{s'}^\Delta \cdot \Gamma_{p,q}^{++}\} V(\mathbf{k}) = \\
&= -3\frac{1}{3} \text{Tr}\{\sigma^i \Gamma_{q-k, p-k}^{++} \sigma^j \Gamma_{p,q}^{++}\} w_{sc}^i w_{cs'}^j V(\mathbf{k}) = \frac{3}{2} V_\rho^{++} \delta_{ss'}. \tag{4.26}
\end{aligned}$$

To arrive at the results of Eqs.(4.24), (4.25) and (4.26) the diquark is assumed to be in the baryon center of mass. Using a spectroscopic decomposition of the baryon wave function in terms of the harmonic oscillator basis we have numerically checked this approximation to introduce an error which is smaller than 6%. Within this approximation and having the spin×flavor nucleon structure – see Appendix B 2 – in mind, we conclude:

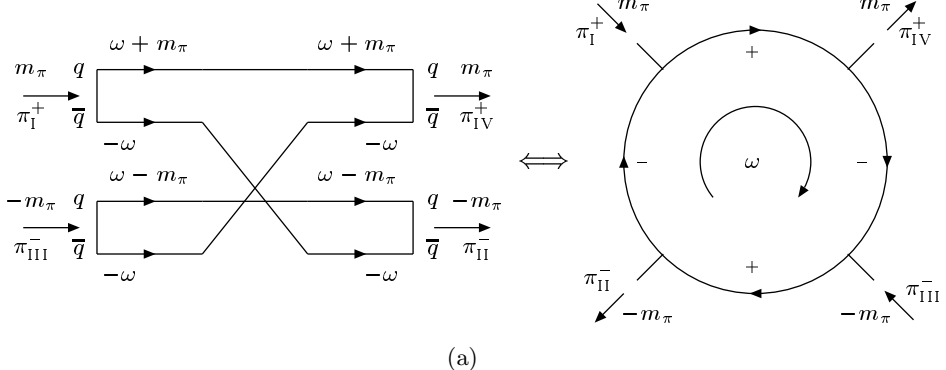
$$\begin{aligned}
V_N^{++} &= \frac{3}{4} (V_\pi^{++} + V_\rho^{++}) \delta_{ss'}, \\
V_\Delta^{++} &= \frac{3}{2} V_\rho^{++} \delta_{ss'}. \tag{4.27}
\end{aligned}$$

## V. FOUR EXTERNAL SOURCES

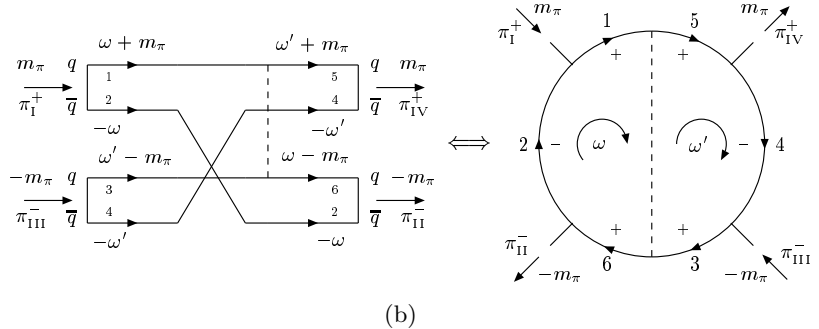
### A. $\pi - \pi$ scattering

In Fig. 6 we show some of the diagrams contributing to  $\pi - \pi$  scattering.  $\{I, II\}$  represent incoming particles whereas  $\{III, IV\}$  represent outgoing particles. In each case we will have two energy-spin Salpeter amplitudes  $\phi^\pm$ . In total there are 48 diagrams plus kinetic energy insertions. The  $\pm$  superscripts in pions  $I \dots IV$  represent the different energy-spin amplitudes. Notice that these diagrams closely resemble those of Fig.4 so that we could anticipate the model independence of  $\pi - \pi$  scattering lengths if the map  $\{\pi \times \pi \rightarrow \pi\}$  respected the structure of the pion Salpeter equation. In Appendix C we show how this mapping can be constructed.

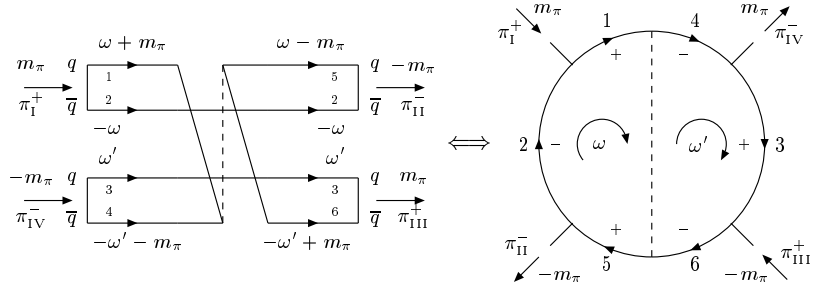
Notice that quark exchange *and* quark annihilation amplitudes are both necessary. Of course this is a consequence of the Dirac nature of quarks but at this stage it is important to state that if we were to have only quark exchange we would only have obtained repulsion. This is precisely the case of exotic scattering [15]. It is the chiral symmetry which produces the right amount of exchange versus annihilation diagrams to produce the Weinberg scattering lengths.



(a)



(b)



(c)

FIG. 6: The left hand side representations are self explanatory. The other representations (ball graph) are the first ones disentangled. The + and - signs stand for the quark and antiquark propagators, respectively.

Notice that in those diagrams we always have for the quark lines an alternation of pluses and minuses, reflecting the way that the Feynman projectors  $\Lambda^\pm$  line up in the Salpeter equation. Repeating the steps we performed for the Salpeter equation, let us consider the energy integrations. First a note on conventions. Throughout the paper we adhere to the following convention: upper case Latin letters represent generic Roman numbers and these are reserved to represent hadrons as a whole, whereas lower case Latin numbers denote the internal quarks and antiquarks.

We have two possible cases in the energy loop integrations. The first case arises when we integrate out, in the diagram 6(a), the energy loop  $w$ , to get a propagator for each pion (here denoted by  $G_0$ ) times the energy flowing in the diagram. We have,

$$i G_{\pi I}^0 G_{\pi II}^0 G_{\pi III}^0 G_{\pi IV}^0 \left( \sum T_i - p_i^0 \right) \quad (5.1)$$

with  $T_i$  denoting the quark  $i$  kinetic term and  $p_i^0$  the energy flowing in that quark;

$$G_{\pi I}^0 = \frac{i}{-E_{IV,I}^+ - E_{I,II}^-}; \quad E_{i,j}^\pm = \pm \frac{p_i^0 - p_j^0}{2} + E(\mathbf{p}_i - \mathbf{p}_j); \quad E(\mathbf{p}_i - \mathbf{p}_j) = \sqrt{(\mathbf{p}_i - \mathbf{p}_j)^2 + m_\pi^2}. \quad (5.2)$$

The second case is illustrated by diagram 6(b). After integration in  $w$  as before, we will get again the same propagators  $G_0$ , now together with a potential term  $V_{13;56}^{++}$  – connecting quark lines 1 and 3 to quark lines 5 and 6 – instead of a

kinetic term,

$$i G_{\pi I}^0 G_{\pi II}^0 G_{\pi III}^0 G_{\pi IV}^0 V_{13;56}^{++}(|\mathbf{k} - \mathbf{k}'|). \quad (5.3)$$

The case of diagram 6(c) yields, upon integration in the energy loop, an expression identical to Eq.(5.3) but now with an annihilation potential  $V_{14;56}^{+-}$  instead of  $V^{++}$ . Again as we have done in Chapter III for the case of two meson sources, i.e mesonic Salpeter equations, we can always associate the individual mesonic propagators  $G^0$  with the Salpeter amplitudes  $\phi^\pm$  to obtain the  $\pi - \pi$   $T$  matrix at zero pion momenta for  $I = \{2, 0\}$ . Upon evaluation of all the potential diagrams plus kinetic insertions we have – see Appendix C,

$$T_{RGM} = 2(\sqrt{2m_\pi})^4 \left(\frac{1}{3}\right)_{\text{color}} \left(\frac{1}{2}\right)_{\text{spin}} \left( a_I [\phi^{-2}, \phi^{+2}] H_\pi \begin{bmatrix} \phi^{+2} \\ \phi^{-2} \end{bmatrix} + b_I [\phi^+ \phi^-, \phi^+ \phi^-] H_\pi \begin{bmatrix} \phi^+ \phi^- \\ \phi^+ \phi^- \end{bmatrix} + c_I [\phi^{+2}, \phi^{-2}] (H_\pi - \sigma_3 m_\pi) \begin{bmatrix} \phi^{+2} \\ \phi^{-2} \end{bmatrix} \right), \quad (5.4)$$

where RGM stands for Resonating Group Method. In Ref.[10] it was shown that the infinite sum of ladder diagrams containing kernel insertions of the type shown in Fig.3(a) and 3(d) is *equivalent* to an RGM calculation *provided* we use Salpeter amplitudes for the incoming and outgoing hadronic wave functions. To go beyond RGM one needs to consider the vertices 3(b) and 3(c). This will lead to effective mesonic exchanges between quarks. This is a general feature for the hadronic scattering in the instantaneous interaction and therefore applies both to  $\pi - \pi$  and  $\pi - N(\Delta)$  scattering.

In Eq.(5.4) integration in the quark loop momenta is assumed.  $H_\pi$ , the Hamiltonian is given in Eq.(4.19) and the constants  $a_I$ ,  $b_I$  and  $c_I$ , coming the isospin traces are given by – see Appendix B 1,

$$a_{[I=0, I=2]} = [3/2, 0]; \quad b_{[0, 2]} = [3/2, 0]; \quad c_{[0, 2]} = [-1/2, 1]. \quad (5.5)$$

The term  $(\sqrt{2m_\pi})^4$  comes from the normalization of the Salpeter amplitudes – see Appendix A. There is an extra factor of two. This factor is automatically obtained when we draw all possible distinct diagrams. Finally we have the spin and color factors which are trivial. Eqs.(5.4) and (4.19) are exact to order  $m_\pi$ .

Equation (5.4) is extraordinary simple to evaluate in the limit of strong interactions defined as the limit when  $\sin \varphi(k) \rightarrow 1$ . This limit always exists because, as it was seen before, for a given class of the quark kernels (for instance linear confinement) the mass gap equation for  $\varphi(k)$  can always be cast as a dimensionless equation for  $\varphi(k/K_0)$  for an arbitrary kernel strength  $K_0$ . The strong limit is given by  $K_0 \rightarrow \infty$ . This limit is *enough* to obtain the Weinberg results for the scattering lengths. To see this, it is enough to use Eq.(4.13) to obtain,

$$\int [\phi^+, \phi^-] \sigma_3 \begin{bmatrix} \phi^+ \\ \phi^- \end{bmatrix} = \int 4 \sin \varphi \Delta = 1; \quad \int [\phi^-, \phi^+] \sigma_3 \begin{bmatrix} \phi^{+2} \\ \phi^{-2} \end{bmatrix} = \int 2 \sin^2 \varphi \Delta = \frac{1}{2a} \quad (5.6)$$

and so on. Then, using Eqs. (4.17, 4.18), it is a text book calculation to obtain in the lowest order in  $m_\pi$ , the  $\pi - \pi$  scattering lengths from the  $T$  matrix, Eq.(5.4). It is just the Born approximation  $T_{RGM} = 16\pi m_\pi a_s RGM \Rightarrow a_s RGM = (-m_{red}/(2\pi))(T_{RGM}/(\sqrt{2m_\pi})^4)$ . We obtain the RGM  $\pi - \pi$  scattering lengths in the point-like limit,

$$a_s^{I=0} RGM = \frac{7}{32\pi} \frac{m_\pi}{f_\pi^2}, \quad a_s^{I=2} RGM = -\frac{1}{16\pi} \frac{m_\pi}{f_\pi^2}. \quad (5.7)$$

At this stage two questions need to be answered. The first question dwells whether the results of Eq.(5.7) hold when we go beyond RGM and consider, *still in the point-like limit*, the *set of all possible diagrams* which is larger than the class of diagrams (already containing an infinite number of diagrams) considered so far. The answer is yes.

Finally we have the question of whether the results of Eq.(5.7) still hold *when we relax the point-like limit*. Again the answer is yes. Both issues will be considered in Chapter VI.

## VI. GOING BEYOND RGM EQUATIONS: INTERMEDIATE EXCHANGE OF MESONS

### A. Coupling hadrons to quarks and antiquarks

So far we have not used two of the four microscopic basic diagrams shown in figure 3. These two remaining diagrams – Fig.3(b) and 3(c) – can only enter in hadronic reactions through either the coupling  $Z_q$  depicted in Fig. 7 or the

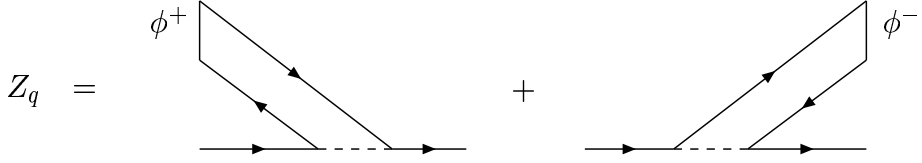


FIG. 7: Coupling of a meson to two quarks

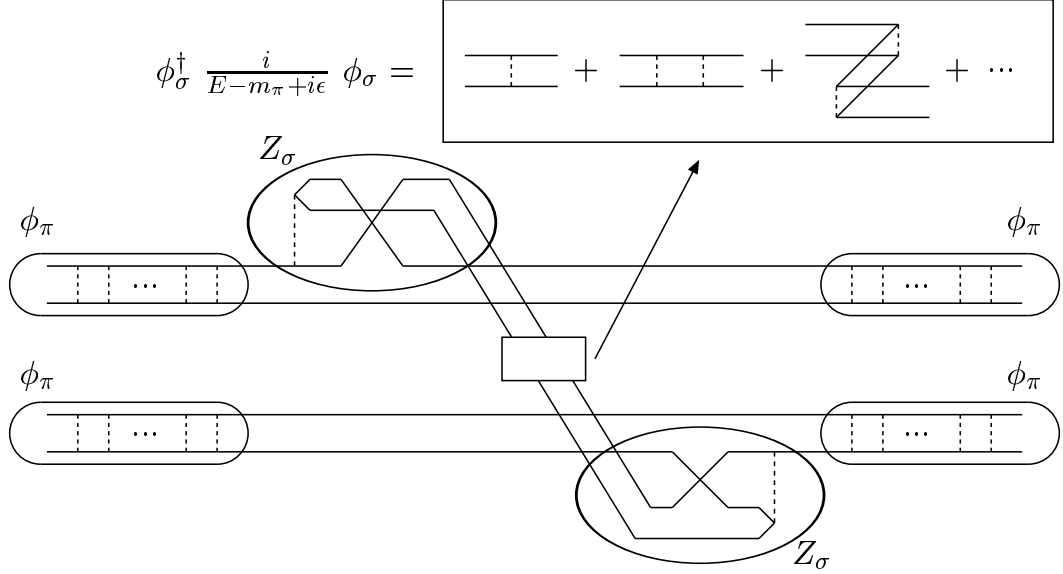


FIG. 8: Diagrams with  $\sigma$  exchange coupling. Notice that the intermediate  $\sigma$  ladders sum to give  $\phi_\sigma^\dagger i/(E - M_\sigma + i\epsilon) \phi_\sigma$ .

corresponding coupling for the antiquarks,  $Z_{\bar{q}}$ , which has the same structure. Using the Feynman rules we have for  $Z_q$ ,

$$(Z_{[\mathcal{M}] q})_{\alpha\beta} = \int \frac{d^4 p'}{(2\pi)^4} \frac{m}{E_q(\mathbf{p}')} \left[ \frac{\Gamma_{\alpha\mu}^{++} \phi_{\mu\nu}^{+ [\mathcal{M}]}(M, \mathbf{p}') \Gamma_{\nu\beta}^{-+}(-i\mathcal{K}(\mathbf{p} - \mathbf{p}'))}{((M/2 + w) - E_q(\mathbf{p}') + i\epsilon)((-M/2 - w) - E_q(-\mathbf{p}') + i\epsilon)} + \frac{\Gamma_{\alpha\mu}^{+-} \phi_{\mu\nu}^{- [\mathcal{M}]}(-M, \mathbf{p}') \Gamma_{\nu\beta}^{++}(-i\mathcal{K}(\mathbf{p} - \mathbf{p}'))}{((-M/2 - w) - E_q(-\mathbf{p}') + i\epsilon)((-M/2 + w) - E_q(\mathbf{p}') + i\epsilon)} \right] \quad (6.1)$$

and a similar expression for  $Z_{\bar{q}}$ . In Eq.(6.1) it is described the coupling of an arbitrary meson  $\mathcal{M}$ ,  $\phi^{\pm [\mathcal{M}]}$ , to a quark line. Prominent examples of such couplings are the pion and  $\sigma$  coupling to quarks. Of course other mesonic couplings are possible. These  $Z_q$  and  $Z_{\bar{q}}$  couplings may appear in  $\pi - \pi$  scattering only through the way shown in Fig.8. We have exhausted all the microscopic quark interactions depicted in figure 3. Therefore for  $\pi\pi$  scattering (as well as for any other hadron-hadron scattering) we can have, for the Hamiltonian of Eq.(2.1) only three classes of diagrams as shown in Fig.9. The first class (class A) contains the infinite set of diagrams which have already been considered to obtain the results of Eq.(5.7). They have the common property of having no intermediate exchange of color singlets (hadrons): they are 1-hadron irreducible diagrams. Class B contains all diagrams having the exchange, in the s-channel, of one hadron (represented for the case of  $\pi\pi$  by a  $\sigma$  exchange). Class C and D are analogous to class B with exchanges being made in the t and u channels. The  $\sigma$  besides being a scalar particle with the lowest mass and therefore the most relevant exchange for the evaluation of  $\pi - \pi$  low energy  $T$  matrix also plays – as it will be shown later – a singular role in enforcing global chiral symmetry for the  $T$  matrix. Any Feynman diagram can be thought as a combination of these skeletons.

Notice that in Eq.(6.1) we always have products like  $\Gamma^{++}\Gamma^{-+}$  or  $\Gamma^{+-}\Gamma^{++}$ . Using the definitions of Eq.(4.4) and the quark vertices defined in Appendix B it is not hard to see that both  $Z_q$  and  $Z_{\bar{q}}$  couplings go to zero in the point-like limit  $\varphi(k) \rightarrow \pi/2$  irrespective of the actual meson being coupled to the quarks. To see this it is enough to consider

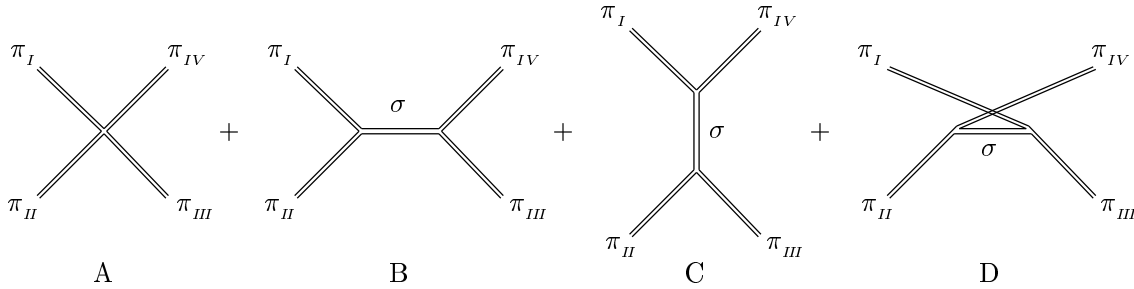


FIG. 9:

the definitions of  $\Gamma^{\pm\pm}$ , Eq.(4.4). Then it is not hard to see that both numerators of Eq.(6.1) contain products like,

$$Z_{[\mathcal{M}]} q \propto u^\dagger \beta \Gamma u \dots u^\dagger \beta \Gamma v . \quad (6.2)$$

In Table III these vertices are given for the two possible Dirac vertices  $\beta$  and  $\gamma$ . For the Dirac vertex equal to  $\beta$  we have that  $\Gamma^{+-}$  and  $\Gamma^{-+}$  go to zero when  $\varphi(k) \rightarrow \pi/2$ .  $\Gamma^{++}$  remain finite. It is the other way around for the Dirac vertex  $\gamma$ : in this case  $\Gamma^{++} \rightarrow 0$  whereas  $\Gamma^{+-}$  and  $\Gamma^{-+}$  remain finite. In either case  $Z_{[\mathcal{M}]} q \rightarrow 0$  in the point-like limit ( $\varphi(k) \rightarrow \pi/2$ ). This is a general result independent of both the particular kernel used and the coupling meson  $[\mathcal{M}]$ .

Let us examine in detail how  $Z_q$  and  $Z_{\bar{q}}$  enter in  $\pi - \pi$  scattering. Again the arguments for  $\pi - \pi$  can be trivially extended to any hadronic scattering. The simplest new diagrams containing  $Z_q$  and  $Z_{\bar{q}}$  are depicted in figure 10. Notice the appearance in the corresponding leftmost diagrams of two consecutive + (or -) adjacent to each pion, in contradistinction with the diagrams of figure 6. This signals the nature of the Z couplings. Performing the integration in the loop energy  $w$  we get a propagator that can be seen as the beginning of a ladder series for an intermediate particle. For instance, for diagrams (a) and (b) we have, respectively,

$$-G_{\pi III}^0 G_{\pi IV}^0 \frac{i}{-E_{III,IV}^- - E_{I,II}^+}, \quad -G_{\pi II}^0 G_{\pi IV}^0 \left( \frac{i}{-E_{I,II}^- - E_{III,IV}^+} + \frac{i}{-E_{IV,I}^+ - E_{II,III}^-} \right) . \quad (6.3)$$

By adding potential diagrams we can build a ladder of interactions for that intermediate particle and using Eq.(4.16) we get the pole for this intermediate particle – see Fig. 8. Because of G parity we have no three pion couplings so that the largest contribution for the scattering is given by the lowest mass possible intermediate particle, the  $\sigma$  (cf. Fig.9). Clearly, the diagram of figure 10(a) will belong to class B whereas diagram 10(b) will contribute to both Class B and C. Therefore the Y-shaped interaction used in the  $\sigma$  exchange diagrams has the structure presented in Fig.11. In what concerns the  $Y$  couplings, we need only to consider  $Z_{\sigma q, \bar{q}}$ , because the  $Z_{\pi q, \bar{q}}$  vanishes in the chiral limit,

$$Z_{\pi ss'}(k) = 2a \int \frac{d^3 k}{(2\pi)^3} \Gamma^{\pm\pm} \Delta(k') \frac{i\sigma_2}{\sqrt{2}} \Gamma^{-\pm} V(k - k') . \quad (6.4)$$

We get,

$$T_{\sigma \text{ exchange}} = -2(\sqrt{2m_\pi})^4 \left( \frac{1}{2} \right)_{\text{spin}} \left( \frac{1}{3} \right)_{\text{color}} \sum_{\sigma} (a_I + b_I + c_I) (\phi\phi, \phi\phi) \begin{bmatrix} \frac{Z_q^2}{M_\sigma} & \frac{Z_q^2}{M_\sigma} \\ \frac{Z_q^2}{M_\sigma} & \frac{Z_q^2}{M_\sigma} \end{bmatrix} \begin{pmatrix} \phi\phi \\ \phi\phi \end{pmatrix} ; \phi = \phi^{\pm} . \quad (6.5)$$

Now *in the point-like limit* both  $Z_q$  and  $Z_{\bar{q}} \simeq \cos(\varphi(k)) \rightarrow 0$  and therefore all diagrams containing  $\sigma$  exchanges vanish,  $T_{\sigma \text{ exchange}} \rightarrow 0$ ;  $T = T_{RGM} + T_{\sigma \text{ exchange}} \rightarrow T_{RGM}$ . So we have demonstrated that the results of Eq.(5.7) hold, in the point-like limit, for the totality of Feynman diagrams up to  $\sigma$  exchange. We are left to prove this result to hold *even when we go outside the point-like limit*. This will be done in the next subsection.

## B. Proving the Weinberg Theorem beyond the point-like limit

For the purpose of proving that the results embodied in Eqs. (5.7) hold, even when we abandon the point-like limit, it is convenient to use the axial Ward identity to define the dressed axial vertex  $\Gamma_A$  as,

$$\Gamma_A(k_1, k_2) = S^{-1}(k_1)\gamma_5 + \gamma_5 S^{-1}(k_2) , \quad (6.6)$$

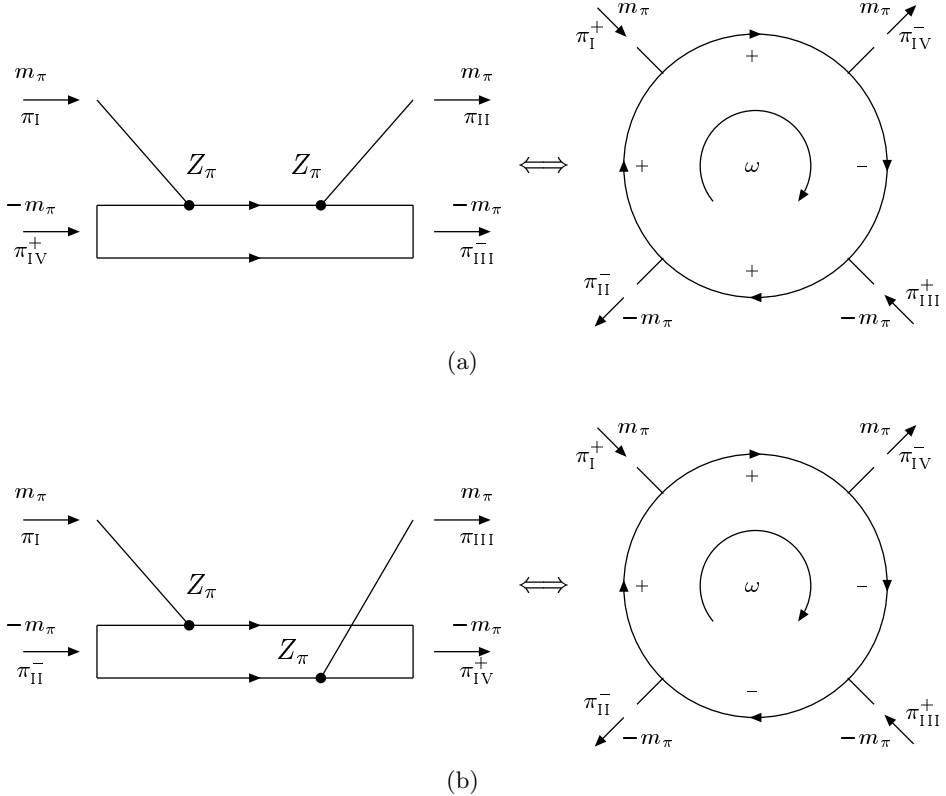


FIG. 10: Some of the diagrams needed for  $\pi - \pi$  scattering.

$$\begin{array}{c} \pi_I \\ \diagup \quad \diagdown \\ \text{Y-shaped vertex} \\ \diagdown \quad \diagup \\ \pi_{II} \end{array} = \phi_{\pi_{II}} \begin{array}{c} q \quad \bar{q} \\ \text{---} \\ \bar{q} \end{array} \phi_\sigma + \phi_{\pi_{II}} \begin{array}{c} q \quad \bar{q} \\ \text{---} \\ \bar{q} \quad \bar{q} \end{array} \phi_\sigma + \text{cyclic permutations}$$

FIG. 11:

where we momentarily leave the Goldstone diagram formalism and revert to the Feynman formalism of Dirac quarks.  $S = i/(A(k) \not{k} + B(k))$  is the dressed quark propagator. The dressed axial vertex  $\Gamma_A$  has the crucial property,

$$\begin{array}{c} \text{Diagram 1} \\ \text{Diagram 2} \end{array} = \gamma_5 \begin{array}{c} \text{Diagram 3} \end{array} + \begin{array}{c} \text{Diagram 4} \end{array} \gamma_5$$

(6.7)

which constitutes a Ward identity for the ladder. In Eq.(6.7) we have introduced  $S^{-1}$  to represent the lower quark propagator  $S$  as the product  $S = SS^{-1}S$ . As it was represented in figure 8, the square box stands for a ladder of quark kernel insertions. To derive Eq. (6.7) it is enough to use Eq.(6.6) together with the fact that the anticommutator of  $\gamma_5$  with the Dirac vertex  $\gamma^\mu$  of the microscopic quark interaction described in Eq.(2.1) vanishes. In this way we are able to translate the  $\gamma_5$  to the extremities of the ladder.

Moreover the dressed axial vertex  $\Gamma_A$  and the pion Bethe-Salpeter vertex  $\chi$  are related to each other in zeroth order of  $P^\mu$  as,

$$\chi = \left[ \frac{i\Gamma_A}{2f_\pi} + \mathcal{O}(P^\mu, m_\pi) \right] , \quad (6.8)$$

where  $f_\pi$  plays the role of a norm. To see this it is enough to compare the equation for the axial vertex  $\Gamma_A$  with the Salpeter equation for the pion,

$$\begin{aligned}\Gamma_A(k_1, k_2) &= \gamma_A(k_1, k_2) + \int \frac{d^4 p}{(2\pi)^4} V S(k_1 + p) \Gamma_A S(k_2 + p) V \mathcal{K}(p) , \\ \chi(k_1, k_2) &= \int \frac{d^4 p}{(2\pi)^4} V S(k_1 + p) \chi S(k_2 + p) V \mathcal{K}(p) ,\end{aligned}\quad (6.9)$$

where the bare vertex  $\gamma_A(k_1, k_2)$  obeys the same Ward identity as in Eq.(6.6), now with the bare quark propagator  $S_0 = i/(\not{k} + m)$  instead of the full quark propagator  $S$ ,

$$\begin{aligned}\gamma_A(k_1, k_2) &= S_0^{-1}(k_1) \gamma_5 + \gamma_5 S_0^{-1}(k_2) , \\ \gamma_A &= \frac{P - 2m}{i} \gamma_5 , \quad P = k_1 - k_2 .\end{aligned}\quad (6.10)$$

Now from Eq.(6.10) we see that  $\gamma_A(k_1, k_2)$  vanishes when both the current quark mass  $m$  and the total pion momentum  $P$  go to zero whereas the dressed vertex  $\Gamma_A$ ,

$$\Gamma_A(k_1, k_2) = \frac{[A(k_1)k_1 - A(k_2)k_2] - [B(k_1) + B(k_2)]}{i} \gamma_5 , \quad (6.11)$$

remains finite in this limit. This sets Eq.(6.8).

The  $\pi - \pi$  scattering amplitude  $T(m_\pi, f_\pi)$  is given by,

$$-i T(m_\pi, f_\pi) = \begin{array}{c} \text{square box} \\ \text{with} \\ \text{two} \\ \text{chi} \\ \text{loops} \end{array} + \begin{array}{c} \text{square box} \\ \text{with} \\ \text{two} \\ \text{chi} \\ \text{loops} \end{array} - \begin{array}{c} \text{square box} \\ \text{with} \\ \text{two} \\ \text{chi} \\ \text{loops} \end{array} . \quad (6.12)$$

In Eq.(6.12), the square boxes stand for a ladder of kernel insertions, so that this equation includes all the Feynman diagrams of the classes A, B and C of figure 9. To proceed further we have to use Eq.(6.8) to expand the  $\chi$ 's in terms of  $\Gamma_A$ 's keeping terms up to order  $P^2$  and  $m_\pi^2$ . Below we will consider in detail one of such terms: three  $\Gamma_A$  and one  $\chi$   $T_{\chi\Gamma_A\Gamma_A}(m_\pi, f_\pi)$ . To this order in  $P^2$  and in  $m_\pi^2$  we would also have to consider three other terms. One containing four  $\Gamma_A - T_{\Gamma_A\Gamma_A\Gamma_A}(m_\pi, f_\pi)$  – another one having two adjacent  $\chi - T_{\chi\chi\Gamma_A}(m_\pi, f_\pi)$  – and a third term where the  $\chi$ 's are non-adjacent  $T_{\chi\Gamma_A\chi\Gamma_A}(m_\pi, f_\pi)$ . No other terms are necessary. The final result is obtained by summing these four types of contributions. When necessary we use Eq.(6.9) to represent  $\Gamma_A$  as follows,

$$\begin{array}{c} \text{square box} \\ \text{with} \\ \text{one} \\ \text{chi} \\ \text{loop} \end{array} \gamma_A = S \Gamma_A S \quad (6.13)$$

and then use the axial Ward identity of Eq.(6.7) to reduce the number of  $\Gamma_A$  vertices in Eq.(6.12),

$$\begin{aligned}\begin{array}{c} \text{square box} \\ \text{with} \\ \text{two} \\ \text{chi} \\ \text{loops} \end{array} &= \begin{array}{c} \text{square box} \\ \text{with} \\ \text{one} \\ \text{chi} \\ \text{loop} \end{array} \Gamma_A S^{-1} \gamma_A \\ &= \gamma_5 \begin{array}{c} \text{square box} \\ \text{with} \\ \text{one} \\ \text{chi} \\ \text{loop} \end{array} \Gamma_A + \begin{array}{c} \text{square box} \\ \text{with} \\ \text{one} \\ \text{chi} \\ \text{loop} \end{array} \gamma_5 \gamma_A .\end{aligned}\quad (6.14)$$

Let us see how this works in the case of  $T_{\chi\Gamma_A\Gamma_A\Gamma_A}$ .

### 1. The $\chi\Gamma_A\Gamma_A\Gamma_A$ amplitude

We have,

$$-i T_{\chi\Gamma_A\Gamma_A\Gamma_A}(m_\pi, f_\pi) = \frac{1}{8f_\pi^3} \left[ \begin{array}{c} \text{square box} \\ \text{with} \\ \text{two} \\ \text{chi} \\ \text{loops} \end{array} \begin{array}{c} \text{square box} \\ \text{with} \\ \text{one} \\ \text{chi} \\ \text{loop} \end{array} \begin{array}{c} \text{square box} \\ \text{with} \\ \text{one} \\ \text{chi} \\ \text{loop} \end{array} \right] \quad (6.15)$$

In Eq.(6.15) the minus signs of  $P_{III}$  and  $P_{IV}$  are consistent with the arrow directions of figure (B4). Now we use Eq.(6.14) to reduce the number of  $\Gamma_A$ . We have,

$$-i T_{\chi \Gamma_A \Gamma_A \Gamma_A} (m_\pi, f_\pi) = \frac{1}{8f_\pi^3} \left[ \frac{\chi P_I}{\Gamma_A P_{II}} * \gamma_A[-P_{IV}] \gamma_5[-P_{III}] + \frac{\Gamma_A[-P_{IV}]}{\chi P_I} * \gamma_5[-P_{III}] \gamma_A P_{II} \right] \quad (6.16)$$

and this is an exact result. To proceed further we use the following trivial identity,

$$\begin{aligned} \text{Diagram: } &= |\chi\rangle \frac{i}{P^2 - m_\pi^2} \langle \chi| \\ \text{Diagram: } &= \chi \frac{i}{P^2 - m_\pi^2} \langle \chi| \chi \rangle \end{aligned} \quad (6.17)$$

where  $P$  denotes the total momenta of the ladder bound state, to rewrite  $\chi$  as follows,

$$\chi = \frac{P^2 - m_\pi^2}{i\langle \chi | \chi \rangle} \text{Diagram: } \chi \quad (6.18)$$

so that we can use again Eq.(6.14) to obtain,

$$\begin{aligned} -i T_{\chi \Gamma_A \Gamma_A \Gamma_A} (m_\pi, f_\pi) &\simeq \frac{1}{8f_\pi^3} \left[ \frac{P_I^2 - m_\pi^2}{2i\langle \chi | \chi \rangle} \{ \chi, \gamma_5 \} * \text{Diagram: } \{ \gamma_A, \gamma_5 \} \right. \\ &\quad \left. + \frac{P_I^2 - m_\pi^2}{i\langle \chi | \chi \rangle} \chi P_I * \text{Diagram: } \gamma_A[-P_{IV}] \gamma_5[-P_{III}] \gamma_5 P_{II} \right. \\ &\quad \left. + \gamma_5[-P_{IV}] \gamma_5[-P_{III}] \gamma_A P_{II} \right]. \end{aligned} \quad (6.19)$$

In Eq.(6.19) we got a ladder inserted between the scalar sources  $\{ \chi, \gamma_5 \}$  and  $\{ \gamma_A, \gamma_5 \}$  and a ladder for the pseudoscalar source  $\chi P_I$ . Due to Eq.(6.10), the scalar term  $\{ \gamma_A, \gamma_5 \}$  contains a term proportional to  $(P - 2m)$  (notice that due to the Gell-Mann-Oakes-Renner relation,

$$\begin{aligned} \int \text{tr}\{S\} &= -i\langle \psi \bar{\psi} \rangle \\ m \int \text{tr}\{S\} &= if_\pi^2 m_\pi^2 \end{aligned} \quad (6.20)$$

the quark mass  $m$  is also proportional to  $m_\pi$ ) to be multiplied by the overall factor  $P^2 - m_\pi^2$ . Hence we will get terms proportional to  $P^3, P^2 m_\pi, P m_\pi^2$  and  $m_\pi^3$ . For small enough pion mass and momenta these terms can be neglected when compared with the terms coming out from the ladder for the pseudoscalar source which are exclusively  $-$  as we will see shortly in Eq.(6.21) – of order  $P^2$  and  $m_\pi^2$ . Therefore we neglect the scalar contributions and use again Eq.(6.18), this time to get rid of the ladder, to obtain,

$$\begin{aligned} -i T_{\chi \Gamma_A \Gamma_A \Gamma_A} (m_\pi, f_\pi) &= \frac{1}{8f_\pi^3} \left[ \chi P_I * \text{Diagram: } \gamma_A[-P_{IV}] \gamma_5[-P_{III}] \gamma_5 P_{II} \right. \\ &\quad \left. + \gamma_5[-P_{IV}] \gamma_5[-P_{III}] \gamma_A P_{II} \right] \\ &= \int \text{tr}\{(S\chi S)_{P_I} (\gamma_A[-P_{IV}] + \gamma_A P_{II})\} / (8f_\pi^3) \end{aligned} \quad (6.21)$$

To evaluate Eq.(6.21) it suffices to consider PCAC,

$$\langle \pi | A_\mu^a | 0 \rangle = \int \text{tr}\{(S\chi S)_{P_I} \gamma^\mu \gamma_5\} = 2f_\pi P^\mu \quad (6.22)$$

and the Gell-Mann Oakes Renner relation in Eq.(6.20), to obtain,

$$\int \text{tr}\{(S\chi S)_{P_I} \gamma_A[-P_{IV}]\} = -2if_\pi(-P_I \cdot P_{IV} + m_\pi^2) \quad (6.23)$$

Applying Eq.(6.23) to Eq.(6.21) we finally get,

$$-i T_{\chi \Gamma_A \Gamma_A \Gamma_A} (m_\pi, f_\pi) = \frac{i}{4f_\pi^2} [-(P_{II} - P_{IV}) \cdot P_I - 2m_\pi^2] \quad (6.24)$$

We have now to consider the three remaining cases:

$$\begin{aligned}
-i T_{\Gamma_A \Gamma_A \Gamma_A \Gamma_A}(m_\pi, f_\pi) &= \left(-\frac{1}{2f_\pi}\right)^4 (8if_\pi^2 m_\pi^2); \\
-i T_{\chi \chi \Gamma_A \Gamma_A}(m_\pi, f_\pi) &= \left(-\frac{1}{2f_\pi}\right)^2 \frac{P_I^2 + P_{IV}^2 - P_I \cdot P_{IV} - P_I \cdot P_{III} - P_{II} \cdot P_{IV} - 2m_\pi^2}{i} \\
-i T_{\chi \Gamma_A \chi \Gamma_A}(m_\pi, f_\pi) &= \left(-\frac{1}{2f_\pi}\right)^2 \frac{P_I^2 + P_{III}^2 - 2m_\pi^2}{i}.
\end{aligned} \tag{6.25}$$

Summing the four T's of Eqs. (6.24) and (6.25) we get,

$$T(m_\pi, f_\pi) = -\frac{1}{4f_\pi^2} [(P_I - P_{IV})^2 + (P_I + P_{II})^2 - 2m_\pi^2], \tag{6.26}$$

where the momentum conservation condition,  $\sum_i P_i = 0$ , was used to simplify the result.

To get the  $\pi - \pi$  scattering amplitude we have to match the external pions, both the incoming pion pair and the outgoing pion pair, with the four pion vertices in the loop diagrams we have just computed. There are six topologically different combinations of the external legs. Now including the flavor traces, and using the Mandelstam relativistic invariant variables,  $s = (P_I + P_{II})^2$ ,  $t = (P_I + P_{IV})^2$  and  $u = (P_I + P_{III})^2$  we finally get for the S-wave scattering amplitudes of  $I = 0$  and  $I = 2$ ,

$$\begin{aligned}
T_{I=0} &= -\frac{3s + t + u - 5m_\pi^2}{2f_\pi^2} \\
T_{I=2} &= -\frac{t + u - 2m_\pi^2}{2f_\pi^2},
\end{aligned} \tag{6.27}$$

which constitutes the Weinberg theorem for  $\pi - \pi$  scattering. For all pion momenta equal to zero Eq.(6.27) yields the scattering lengths of Eq.(5.7):  $a_I([\mathbf{P}_I, \mathbf{P}_{II}, \mathbf{P}_{III}, \mathbf{P}_{IV}] = [0, 0, 0, 0]) = a_{I, RGM}([0, 0, 0, 0])$  regardless both of the confining scale  $K_0$  and the s, t, u exchange of sigmas. This result is easily understood if one first notices that chiral symmetry precludes any scalar contributions independently of the confining scale ( $K_0$ ). Then the remaining contribution for the scattering length,  $a_{RGM}(K_0)$ , can be parameterized in all generality as

$$a_{RGM}^I(K_0) = C_I \frac{m_\pi(K_0)}{f_\pi^2(K_0)} \left( 1 + \sum_X c_X^I \left( \frac{M_X}{K_0} \right)^{\alpha_X} + \sum_{YZ} d_{YZ}^I \left( \frac{M_Y}{K_0} \right)^{\alpha_Y} \left( \frac{M_Z}{K_0} \right)^{\alpha_Z} + \dots \right) : C_{I=0,2} = \frac{7}{32\pi}, -\frac{1}{16\pi} \tag{6.28}$$

In Eq.(6.28)  $M_{X,Y,Z}$  are arbitrary masses and  $c_X^I$ ,  $d_{YZ}^I$  dimensionless coefficients. It turns out that for the class of Hamiltonians of Eq.(2.1) all quantities with dimension of mass  $M_X$  (in the  $\pi - \pi$  case,  $m_\pi$ ,  $f_\pi$  and any other hadronic mass calculated within the model) scale linearly with  $K_0$ . This implies that the multiplicative renormalization  $1 + \sum_X c_X^I M_X / K_0 + \dots$  does not depend on  $K_0$ . Then Eq.(6.28) together with its point-like limit,  $a_{RGM}^I(\infty) = C_I m_\pi(\infty) / f_\pi^2(\infty)$ , of Eq.(5.7), shows it must be 1. Therefore the Hamiltonian formalism complies with the Weinberg theorem independently of the model and of the point-like limit. The point-like limit turns out to be the simplest way to sum *all* the diagrams leading to the Weinberg  $\pi - \pi$  scattering lengths. This simplicity arises from the fact that these scattering lengths do not depend on the actual form of the quark kernel and the fact that, in this limit, *all the diagrams containing  $Z_q$  or  $Z_{\bar{q}}$  vanish*. Leaving the point like limit reintroduces the sigma mediated interactions discussed in Chapter VI-A. These interactions, because sigma is a scalar, coupling directly to a quark (or an antiquark), introduce an effective scalar interaction among quarks which *explicitly* violates chiral symmetry. The  $\bar{\psi}\sigma\Psi$  coupling breaks explicitly chiral invariance. Because we started with a chiral symmetric Hamiltonian the appearance of such terms would have led us to an apparent paradox. The solution is quite simple: outside the point like limit the diagrams of Class A must develop a scalar quark interaction to cancel exactly such scalar interactions arising from the diagrams of Class B and C. This, as we have just seen, is ensured by the Ward identities – the guarantors that we do not leave chiral symmetry. This is, of course, a general feature extensible to *all* hadronic reactions.

In this way we are led to derive a new constraint to the coupling  $Z_\sigma$  of a scalar meson to a quark. Bringing together Eqs.(4.20, 6.5), we get,

$$\int \phi^2 \left( H_\pi^{++} + H_\pi^{+-} - 2 \sum_\sigma \frac{Z_\sigma^2}{m_\sigma^2} \right) \phi^2 = 0. \tag{6.29}$$

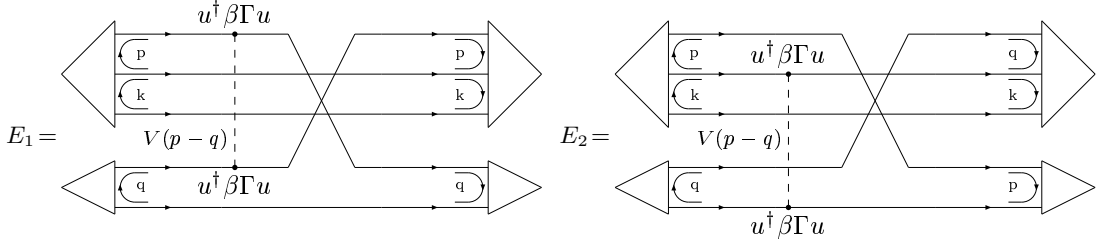


FIG. 12: exchange diagrams

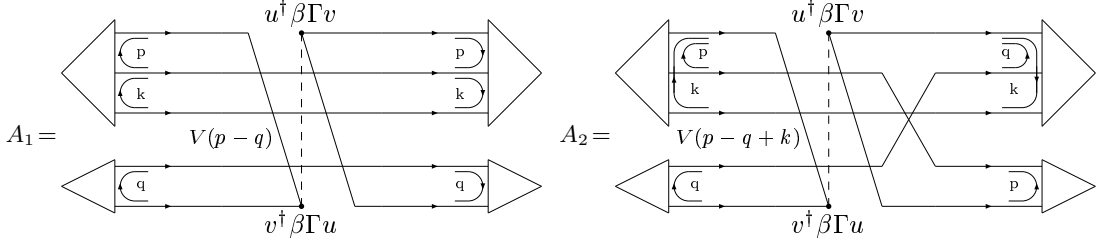


FIG. 13: annihilation diagrams

This result complements the pion Salpeter equation in the chiral limit,  $\int \sin \varphi (H^{++} + H^{+-}) \sin \varphi = 0$ . From eq.(6.29), one sees that the Ward identity ensures that the mass of the lowest scalar should be proportional to its width (excited scalar states are killed by geometric overlaps) *in order to cancel the quark-quark scalar interactions*. With Eq.(6.29) we conclude the detailed study of  $\pi - \pi$ . In the remainder of this paper we will adopt the following principles we have just worked out in detail for the case of  $\pi\pi$ :

*I - For a chiral symmetric Hamiltonian, all effective quark-quark scalar interactions must cancel.*

*II - To do that economically it suffices to use the point-like limit.*

## VII. $\pi - N(\Delta)$ SCATTERING

### A. The RGM (direct coupling) diagrams analogous to the class A $\pi - \pi$ diagrams

In this Chapter we will follow closely the steps used to derive the  $\pi - \pi$  scattering lengths. Some definitions needed for this Chapter are given in appendix A. In Figs. 12, 13 and 14 we depict examples of the 1-baryon and 1-pion irreducible diagrams, needed to build the complete RGM  $T_{\pi N(\Delta)}$  matrix. The diagrams  $E_1$  and  $E_2$  are the usual Resonating Group Diagrams yielding for most reactions, a repulsive force. This is the case of NN elastic scattering where they are shown to provide a substantial repulsion [17]. The same happens with exotic meson-meson reactions. Retrospectively we can say that the success of the present calculation constitutes an extension of these old results. The diagram  $A_1$  contains quark-antiquark annihilation amplitudes and for most cases it provides for attraction. As it was explained in Ref.[10] the infinite ladder series obtained by multiple insertions of diagrams  $E$ ,  $E_1$ ,  $E_2$ ,  $A_1$  and  $N_3$  will yield a  $T$  matrix which will be identical to the RGM  $T$  matrix, where we need to consider each of the above diagrams only once *provided* the asymptotic hadronic wave functions are given by the respective Salpeter amplitudes. No repeated diagrams are allowed. Diagram  $A_2$  constitutes an example of a repeated diagram ( $E \otimes A_1$ ) and should not be considered for the  $T$  matrix. Provided we keep to color singlets, diagram  $E_1$  is the simplest diagram we can draw because a single kernel insertion (which goes with  $\lambda \cdot \lambda$  in color space) has zero matrix element between color singlets. Therefore contributions like  $A_2$  will not be considered in this paper.

Again, to avoid double counting we have to subtract diagram  $N_3$ , depicted in Fig.5, from diagram E. This is a trivial consequence from the fact that both the incoming and outgoing states contain infinite ladders of kernel insertions. On the other hand the baryon pair of quarks which are not interchanged constitute per se one such ladder. It happens that the rule of composition of one ladder as the product of two identical ladders needs these subtractions in order to avoid double counting of Feynman diagrams. Adding all the diagrams we get for the overlap kernel,

$$\mathcal{O}_K^{\text{RGM}} = \langle N\pi | 3(E - N_3 + E_1 + 2E_2 + A_1) | N\pi \rangle. \quad (7.1)$$

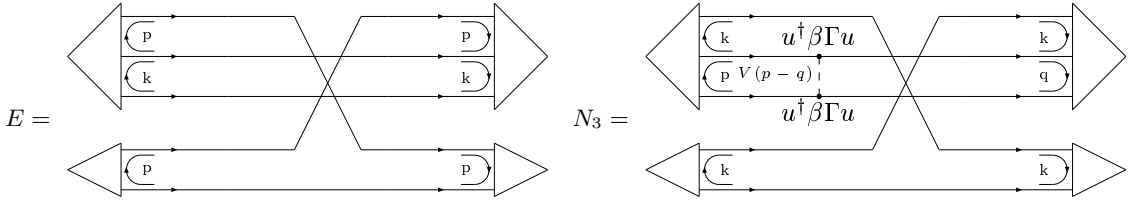


FIG. 14: Double counting diagram

TABLE I: Nucleon Total Contribution. The upper (lower) sum/subtraction signs are associated with  $\phi^+ \otimes \phi^+$  ( $\phi^- \otimes \phi^-$ ).

$\mathcal{E}$	$\frac{1}{4}(I \pm \frac{2}{3}\tau_N \cdot \tau_\pi) \sum(T - E)$
$V_{N3}$	$\frac{1}{16}(I \pm 2\tau_N \cdot \tau_\pi)V_\pi^{++}(\mathbf{p}, \mathbf{q}) + \frac{1}{16}(I \mp \frac{2}{3}\tau_N \cdot \tau_\pi)V_\rho^{++}(\mathbf{p}, \mathbf{q})$
$V_{E1}$	$-\frac{1}{4}(I \pm \frac{2}{3}\tau_N \cdot \tau_\pi)V_\pi^{++}(\mathbf{p}, \mathbf{q})$
$V_{E2}$	$-\frac{1}{8}I V_\pi^{++}(\mathbf{p}, \mathbf{q}) - \frac{1}{8}(I \pm \frac{4}{3}\tau_N \cdot \tau_\pi)V_\rho^{++}(\mathbf{p}, \mathbf{q})$
$V_{A1}$	$\frac{1}{4}(I \mp \frac{2}{3}\tau_N \cdot \tau_\pi)V_\pi^{+-}(\mathbf{p}, \mathbf{q})$

The factors 3 and 6 are there to account for all the possible permutations in the exchange of quarks.

It is very easy to calculate the energy loop integrals,

$$\begin{aligned}
 E &\rightarrow -i \left( \sum_{i=1}^5 T_i - E_i \right) G_{i\pi}^0 G_{iN}^0 G_{f\pi}^0 G_{fN}^0, \\
 N_3 &\rightarrow (-i) V_{N3} G_{i\pi}^0 G_{iN}^0 G_{f\pi}^0 G_{fN}^0 (1 + (G_{i\pi}^0)^{-1} G_{167}^0 + (G_{f\pi}^0)^{-1} G_{234}^0), \\
 E_1 &\rightarrow (-i) V_{E1} G_{i\pi}^0 G_{iN}^0 G_{f\pi}^0 G_{fN}^0, \\
 E_2 &\rightarrow (-i) V_{E2} G_{i\pi}^0 G_{iN}^0 G_{f\pi}^0 G_{fN}^0, \\
 A_1 &\rightarrow (-i) V_{A1} G_{i\pi}^0 G_{iN}^0 G_{f\pi}^0 G_{fN}^0,
 \end{aligned} \tag{7.2}$$

where the  $G_{i,f}^0$  represent the hadronic propagators of the initial and final free asymptotic states. For instance  $G_{iN}^0$ , represents the propagator of the initial nucleon,

$$G_{iN}^0 = i(E_1 + E_2 + E_3 - E(p_1 + k) - E(p_2 - k + k') - E(p_3 - k'))^{-1} \tag{7.3}$$

TABLE II: Delta Total Contribution. The upper (lower) sum/subtraction signs are associated with  $\phi^+ \otimes \phi^+$  ( $\phi^- \otimes \phi^-$ ).

$\mathcal{E}$	$\frac{1}{4}(I \pm \frac{2}{3}\tau_\Delta \cdot \tau_\pi) \sum(T - E)$
$V_{N3}$	$\frac{1}{8}(I \pm \frac{2}{3}\tau_\Delta \cdot \tau_\pi)V_\rho^{++}(\mathbf{p}, \mathbf{q})$
$V_{E1}$	$-\frac{1}{4}(I \pm \frac{2}{3}\tau_\Delta \cdot \tau_\pi)V_\pi^{++}(\mathbf{p}, \mathbf{q})$
$V_{E2}$	$-\frac{1}{4}(I \pm \frac{2}{3}\tau_\Delta \cdot \tau_\pi)V_\rho^{++}(\mathbf{p}, \mathbf{q})$
$V_{A1}$	$\frac{1}{4}(I \mp \frac{2}{3}\tau_\Delta \cdot \tau_\pi)V_\pi^{+-}(\mathbf{p}, \mathbf{q})$

and  $G_{167}^0$  a propagator of a “baryon” composed of particles 1, 6 and 7.  $E_i, p_i$  represents the quark i energy and momentum and  $E(\mathbf{q})$  the associated quasi-particle energy. For simplicity of notation let us denote by  $\mathcal{E}$  the operator  $(\sum_{i=1}^5 T_i - E_i)$  and store the results arising from the remaining space integrations and color×spin×flavor traces in the set  $\mathcal{C}=\{\mathcal{E}, V_{N3}, V_{E1}, V_{E2}, V_{A1}\}$ . Naturally the factors 3 and 6 are also included in this set. Let us briefly discuss the steps leading to these results. In the color subspace, the  $N$  and  $\Delta$  wave functions are the same. When it comes to flavor, we know the Nucleon flavor to mix with spin. For the nucleon we have:  $(F_{\text{flavor}}F_{\text{spin}} + D_{\text{flavor}}D_{\text{spin}})/\sqrt{2}$ , whereas for the Delta we have the direct product of the totally symmetric spin and flavor wave functions – see Eq.(B9) for the spin wave functions. In Tables IV and V we present the pion color and flavor results for the set  $\mathcal{C}$ . It is not hard to see that energy conservation forces the pion wave functions to be of the same kind in energy spin: either they are both positive energy components or negative. The color×spin×flavor contributions for all the diagrams of set  $\mathcal{C}$ , are given in Tables I and II, for the products of either two positive or negative energy pion wave functions. Finally, we have to integrate the terms above against the appropriate Salpeter pion wave functions. For example, the  $\pi N$  terms with  $\phi^+ \otimes \phi^+$  are given by,

$$\begin{aligned}
 & \Psi(p, k)\phi^+(k) \left( \frac{1}{16} [I + 2\tau_N \cdot \tau_\pi] V_\pi^{++}(\mathbf{p}, \mathbf{q}) + \frac{1}{16} \left[ I - \frac{2}{3}\tau_N \cdot \tau_\pi \right] V_\rho^{++}(\mathbf{p}, \mathbf{q}) \right) \Psi(q, k)\phi^+(k) \\
 & \Psi(p, k)\Psi(p, k) \left( \frac{1}{4} \left[ I + \frac{2}{3}\tau_N \cdot \tau_\pi \right] V_\pi^{++}(\mathbf{p}, \mathbf{q}) + \frac{1}{4} \left[ I - \frac{2}{3}\tau_N \cdot \tau_\pi \right] V_\pi^{+-}(\mathbf{p}, \mathbf{q}) \right) \phi^+(q)\phi^+(q) \\
 & \Psi(p, k)\phi^+(p) \left( \frac{1}{8} I V_\pi^{++}(\mathbf{p}, \mathbf{q}) + \frac{1}{8} \left[ I + \frac{4}{3}\tau_N \cdot \tau_\pi \right] V_\rho^{++}(\mathbf{p}, \mathbf{q}) \right) \Psi(q, k)\phi^+(q)
 \end{aligned} \tag{7.4}$$

Similarly for  $\Delta$  we have,

$$\begin{aligned}
 & \Psi_\Delta(p, k)\phi^+(k) \left( \frac{1}{8} \left[ I + \frac{2}{3}\tau_\Delta \cdot \tau_\pi \right] V_\rho^{++}(\mathbf{p}, \mathbf{q}) \right) \Psi_\Delta(q, k)\phi^+(k) \\
 & \Psi_\Delta(p, k)\Psi_\Delta(p, k) \left( \frac{1}{4} \left[ I + \frac{2}{3}\tau_\Delta \cdot \tau_\pi \right] V_\pi^{++}(\mathbf{p}, \mathbf{q}) + \frac{1}{4} \left[ I - \frac{2}{3}\tau_\Delta \cdot \tau_\pi \right] V_\pi^{+-}(\mathbf{p}, \mathbf{q}) \right) \phi^+(q)\phi^+(q) \\
 & \Psi_\Delta(p, k)\phi^+(p) \left( \frac{1}{4} \left[ I + \frac{2}{3}\tau_\Delta \cdot \tau_\pi \right] V_\rho^{++}(\mathbf{p}, \mathbf{q}) \right) \Psi_\Delta(q, k)\phi^+(q)
 \end{aligned} \tag{7.5}$$

It is important to perform the momentum integrals. It is straightforward to reorganize the flavor factors multiplying  $V_{\pi\rho}^{\pm\pm}$  (as in Eqs.(7.4,7.5)). In these equations we have terms in  $\tau \cdot \tau$  together with scalar terms (proportional to  $I$ ). These scalar terms, whose presence would have explicitly broke chiral symmetry, will be shown to add up to zero.

Starting in terms with  $V_\pi$  we have only to consider a generic integral like,

$$\begin{aligned}
 \mathcal{J} &= \int \frac{d^3 p}{(2\pi)^3} \int \frac{d^3 q}{(2\pi)^3} A(\mathbf{p})(2T + V_\pi^{++}(\mathbf{p}, \mathbf{q}) + V_\pi^{+-}(\mathbf{p}, \mathbf{q}))B(\mathbf{q}) \\
 &= \frac{1}{2} \begin{bmatrix} A(\mathbf{p}) & A(\mathbf{p}) \end{bmatrix} \begin{bmatrix} 2T + V_\pi^{++}(\mathbf{p}, \mathbf{q}) & V_\pi^{+-}(\mathbf{p}, \mathbf{q}) \\ V_\pi^{+-}(\mathbf{p}, \mathbf{q}) & 2T + V_\pi^{--}(\mathbf{p}, \mathbf{q}) \end{bmatrix} \begin{bmatrix} B(\mathbf{q}) \\ B(\mathbf{q}) \end{bmatrix}
 \end{aligned} \tag{7.6}$$

Where  $A$  and  $B$  contain products of pion and baryon Salpeter wave functions. Now we make the crucial observation

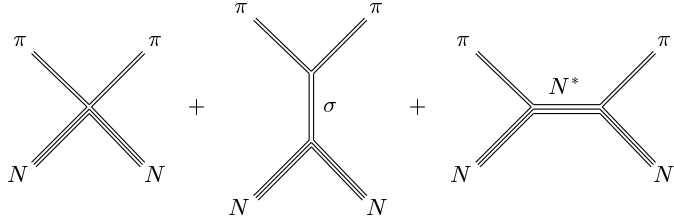


FIG. 15: Classes of diagrams in  $N(\Delta) - \pi$  scattering

that in the pion sector the Hamiltonian can be written as,

$$\begin{bmatrix} 2T + V_{\pi}^{++}(\mathbf{p}, \mathbf{q}) & V_{\pi}^{+-}(\mathbf{p}, \mathbf{q}) \\ V_{\pi}^{-+}(\mathbf{p}, \mathbf{q}) & 2T + V_{\pi}^{--}(\mathbf{p}, \mathbf{q}) \end{bmatrix} = \sum_n \sigma^3 \begin{bmatrix} \phi_n^+(\mathbf{p}) \\ \phi_n^-(\mathbf{p}) \end{bmatrix} m_{\pi}^{(n)} \begin{bmatrix} \phi_n^+(\mathbf{q}) & \phi_n^-(\mathbf{q}) \end{bmatrix} \sigma^3 \quad (7.7)$$

We truncate the above sum to the ground state ( $n = 0$ ), thereby disregarding contributions of excited pion states which are irrelevant for lowest mass pions we are considering, and substitute Eq.(7.7) in Eq.(7.6) to obtain,

$$\mathcal{J} = \frac{1}{2} \int \frac{d^3 p}{(2\pi)^3} A(\mathbf{p})(\phi^+(\mathbf{p}) - \phi^-(\mathbf{p})) m_{\pi} \int \frac{d^3 q}{(2\pi)^3} B(\mathbf{q})(\phi^+(\mathbf{q}) - \phi^-(\mathbf{q})) \quad (7.8)$$

Eq.(7.7) is exact and constitutes the cornerstone of the model. Now if we use Eq.(4.13) for  $\phi^+$  and  $\phi^-$ , we get,

$$\int \frac{d^3 p}{(2\pi)^3} \int \frac{d^3 q}{(2\pi)^3} A(\mathbf{p})(2T + V_{\pi}^{++} + V_{\pi}^{+-}) B(\mathbf{q}) \rightarrow \frac{4}{3} f_{\pi}^2 m_{\pi} \int \frac{d^3 p}{(2\pi)^3} A(\mathbf{p}) \Delta(\mathbf{p}) m_{\pi} \int \frac{d^3 q}{(2\pi)^3} \Delta(\mathbf{q}) B(\mathbf{q}) . \quad (7.9)$$

The remainder of the terms left over when arranging the terms to obtain Eq.(7.7) can be, using Eq.(4.27), cast as,

$$\begin{aligned} \int \frac{d^3 p}{(2\pi)^3} \int \frac{d^3 q}{(2\pi)^3} A(\mathbf{p}) \left( 2T + \frac{1}{2}(V_{\pi}^{++} + V_{\rho}^{++}) \right) B(\mathbf{q}) &\rightarrow \frac{1}{6} \int \frac{d^3 p}{(2\pi)^3} A(\mathbf{p}) \Psi M_N \int \frac{d^3 q}{(2\pi)^3} \Psi B(\mathbf{q}) \\ \int \frac{d^3 p}{(2\pi)^3} \int \frac{d^3 q}{(2\pi)^3} A(\mathbf{p})(2T + V_{\rho}^{++}) B(\mathbf{q}) &\rightarrow \frac{1}{6} \int \frac{d^3 p}{(2\pi)^3} A(\mathbf{p}) \Psi_{\Delta} M_{\Delta} \int \frac{d^3 q}{(2\pi)^3} \Psi_{\Delta} B(\mathbf{q}) \end{aligned} \quad (7.10)$$

We have only to calculate wave function integrals to obtain the  $\pi - N(\Delta)$  overlap kernel, Eq.(7.1).

## B. Going beyond RGM: The one hadron exchange diagrams

As in  $\pi - \pi$  scattering, we can separate the set of  $N(\Delta) - \pi$  Feynman diagrams into three classes – see Fig. 15. Again because of G parity no three pion vertices are allowed. Besides the 1-hadron irreducible diagrams we have considered so far in the figures 12, 13 and 14 and which belong to class 15A, we have two other classes. In class 15C, Feynman diagrams always contain a  $Z_q$  or  $Z_{\bar{q}}$  coupling and, therefore, these diagrams vanish in the point-like limit. Finally, let us consider the 15B class. The first fact that it is important to notice is that the  $\pi NN^*$  vertex has two contributions. One, is a  $Z_{\pi}$  coupling. Again it vanishes in the point-like limit. The other contribution is presented in Fig. 16. We have a quark exchange together with an interaction with a third quark. This coupling also vanishes in the point-like limit. Now, looking once again at Eq.(7.2) we see that diagram  $N_3$  has a contribution to the  $N^*$  class that we can disregard in the point like limit because it is of the  $Z_{\pi}$  kind.

As it happen with the  $\pi - \pi$  scattering case the point like limit for  $\pi - N(\Delta)$  scattering turns out to be an expeditious way of calculating the complete  $T_{\pi - N(\Delta)}$  matrix because it is a limit where all intermediate meson exchange decouple. If we were to leave the point like limit these intermediate mesonic exchanges would have started to contribute to the  $T$  matrix, the direct contribution  $\mathcal{O}_{\mathcal{K}}^{\text{RGM}}$  would have also changed, subject to the Ward identity constraint that total

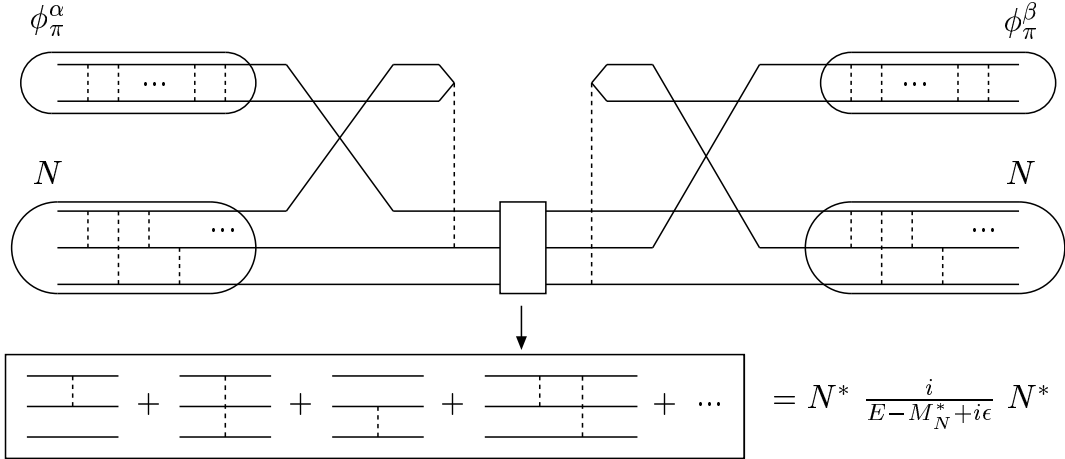


FIG. 16: Odd parity excited nucleon.  $\alpha, \beta$  stand for  $\pm$  Energy signs

scalar contribution *must vanish*. For  $\pi - N(\Delta)$  the equivalent of Eq.(6.29) are,

$$\begin{aligned}
 & \frac{1}{4} \int \Psi(p, k) \Psi(p, k) H_\pi(p, q) \phi(q) \phi(q) + \frac{1}{6} \int \Psi(p, k) \phi(p) (H_N(p, q) - M_N \delta(p - q)) \Psi(q, k) \phi(q) + \\
 & + \frac{1}{12} \int \Psi(p, k) \phi(k) (H_N(p, q) - M_N \delta(p - q)) \Psi(q, k) \phi(k) + g_{\sigma\pi\pi} \frac{1}{M_\sigma} g_{\sigma NN} + (g_{\pi NN^*})^2 \frac{1}{M_{N^*} - M_N} = 0 \\
 & \frac{1}{4} \int \Psi_\Delta(p, k) \Psi_\Delta(p, k) H_\pi(p, q) \phi(q) \phi(q) + \frac{1}{6} \int \Psi_\Delta(p, k) \phi(p) (H_\Delta(p, q) - M_\Delta \delta(p - q)) \Psi_\Delta(q, k) \phi(q) + \\
 & + \frac{1}{12} \int \Psi_\Delta(p, k) \phi(k) (H_\Delta(p, q) - M_\Delta \delta(p - q)) \Psi_\Delta(q, k) \phi(k) + g_{\sigma\pi\pi} \frac{1}{M_\sigma} g_{\sigma\Delta\Delta} + (g_{\pi\Delta\Delta^*})^2 \frac{1}{M_{\Delta^*} - M_\Delta} = 0
 \end{aligned} \tag{7.11}$$

### C. The point like limit

From the discussion of Chapter VII.A we see that we have only to evaluate overlap integrals containing the baryon and pion wave functions. We have to deal with the following integrals,

$$\begin{aligned}
 I_0(\alpha) &= \int d^3 p \Psi \Psi \phi^\alpha \phi^\alpha, \quad I_1(\alpha) = \int d^3 p \Psi \Psi \Psi \int d^3 q \phi^\alpha \phi^\alpha \Psi, \quad I_2(\alpha) = \int d^3 p \Psi \phi^\alpha \Psi \int d^3 q \Psi \phi^\alpha \Psi, \\
 I_3(\alpha) &= \int d^3 p \Psi \Psi \Psi_\Delta \int d^3 q \phi^\alpha \phi^\alpha \Psi_\Delta, \quad I_4(\alpha) = \int d^3 p \Psi \phi^\alpha \Psi_\Delta \int d^3 q \Psi \phi^\alpha \Psi_\Delta, \\
 I_5(\alpha) &= \int d^3 p \Psi \Psi \Delta \int d^3 q \phi^\alpha \phi^\alpha \Delta, \quad I_6(\alpha) = \int d^3 p \Psi \phi^\alpha \Delta \int d^3 q \Psi \phi^\alpha \Delta; \quad \alpha = \pm.
 \end{aligned} \tag{7.12}$$

From the Tables I and II we can see that in some cases we have to sum the above integrals for positive and negative energies, whereas in the other cases we have to subtract them. For example, we have for  $I_0$ ,

$$\begin{aligned}
 I_0(+) + I_0(-) &= \int d^3 p \Psi \Psi \phi^+ \phi^+ + \int d^3 p \Psi \Psi \phi^- \phi^- = \frac{3}{f_\pi^2 m_\pi} \int d^3 p \Psi \Psi (\sin \varphi)^2 + \frac{4}{3} f_\pi^2 m_\pi \int d^3 p \Psi \Psi \Delta^2 \\
 &\approx \frac{3}{f_\pi^2 m_\pi}
 \end{aligned} \tag{7.13}$$

$$\begin{aligned}
 I_0(+) - I_0(-) &= \int d^3 p \Psi \Psi \phi^+ \phi^+ - \int d^3 p \Psi \Psi \phi^- \phi^- = 4 \int d^3 p \Psi \Psi \sin \varphi \Delta \\
 &\approx \frac{1}{N^2}
 \end{aligned} \tag{7.14}$$

where, in the point like limit,  $\Psi \simeq \sin \varphi / N$  and  $N$  is the nucleon/delta wave function normalization.

Using these considerations we can see that the integrals  $I_1, I_2, I_3$  and  $I_4$  in Eq.(7.12) are of the order of  $3/f_\pi^2 m_\pi (1/N^2)$  if they are summed (subtracted) for the positive and negative energies. As for the  $I_5$  and  $I_6$  integrals in Eq.(7.12), they are proportional to  $m_\pi$  which goes to zero in the chiral limit.

In the point like limit the scalar terms (proportional to  $I$ , in Eqs. (7.4,7.5)) are zero,

$$3 I \frac{-\sum E_i + M_N}{4f_\pi^2 m_\pi} = 0 \quad 3 I \frac{-\sum E_i + M_\Delta}{4f_\pi^2 m_\pi} = 0, \quad (7.15)$$

which can be trivially interpreted as the conservation of total energy and coincide with Eqs.(7.11) in this limit.

Putting all the previous results together, the total overlap kernel  $\mathcal{O}_K$  coincides with  $\mathcal{O}_K^{\text{RGM}}$  (no intermediate mesonic exchange) and turns out to be quite simple,

$$\mathcal{O}_K = \mathcal{O}_K^{\text{RGM}} \equiv \frac{4M_N - 2M_\Delta}{9N^2} \tau \cdot \tau_\pi + \mathcal{O}(m_\pi). \quad (7.16)$$

Using the same arguments as in  $\pi - \pi$  it is not hard to see that  $\mathcal{O}_K^{\text{RGM}}$  does not depend, to order zero in  $m_\pi$ , on the scale of confinement. Its dependence on this scale is hidden in the hadron masses and the baryon normalization. The Ward identity of Eq.(7.11) ensures that the scalar contributions for the overlap kernel must vanish independently of such scale. Therefore to order zero in the pion mass the total overlap kernel  $\mathcal{O}_K$  is explicitly independent of the scale we used to evaluate it.

#### D. Derivation of the $\pi N$ and $\pi \Delta$ scattering lengths

In the Born approximation the scattering length is trivial,  $a = -\mu_{\text{red}} \mathcal{O}_K^{\text{RGM}} / (2\pi)$ , and we get,

$$a\{\pi N, \pi \Delta\} = -\frac{m_\pi}{2\pi} \frac{4M_N - 2M_\Delta}{9N^2} \tau \cdot \tau_\pi + \mathcal{O}(m_\pi^2). \quad (7.17)$$

In Eq.(7.17)  $\tau$  is a shorthand notation representing  $\tau_N$  or  $\tau_\Delta$ , whichever is the appropriate case ( $\pi N$  or  $\pi \Delta$ ) and  $\mu_{\text{red}}$  is the reduced  $N\pi$  mass  $\simeq m_\pi$ . The exact result for the scattering lengths would have been given by,

$$a = -\mu_{\text{red}} \mathcal{O}_K^{\text{RGM}} / (2\pi + 2\mu_{\text{red}} \mathcal{O}_K^{\text{RGM}} N^{2/3}). \quad (7.18)$$

In Eq.(7.18)  $\mu_{\text{red}} \approx m_\pi$  and the Born approximation just corresponds to the leading term in  $m_\pi$ . Eq.(7.17) is our result for the scattering length.

## VIII. NUMERICAL RESULTS AND CONCLUSION

We make contact with experimental values for the  $a_{\pi N}\{I = 1/2, 3/2\}$  scattering lengths using a Gaussian form for the nucleon wave function with rms  $\simeq 0.4$  fm. For this rms of we obtain the following values for  $a_{\pi N}$

$$a_{\pi N}\{I = 1/2\} = 0.175 m_\pi^{-1} \quad a_{\pi N}\{I = 3/2\} = -0.087 m_\pi^{-1} \quad (8.1)$$

with a parameters set given by  $\mathcal{S} = \{140 \text{ MeV}, 940 \text{ MeV}, 1230 \text{ MeV}, 93 \text{ MeV}, 1605 \text{ MeV}^{-3/2}, 1605 \text{ MeV}^{-3/2}\}$ . This is, in our point of view, an important result. The Hofstadter charge radius of the nucleon was measured to range between 0.7 fm and 0.8 fm. However it is well known that vector meson dominance should account for most of this charge radius. Therefore it is quite important to measure, without using electromagnetic probes, the hadronic radius of the nucleon. This we have done with the purely hadronic  $\pi - N$  scattering. This hadronic size for the nucleons turns out to be small and this lends some justification to the usage of nucleons as elementary particles in effective N-N forces *provided* we take account of the repulsive core.

With the same parameters set we can predict the  $\pi - \Delta$  scattering lengths,

$$a_{\pi \Delta}\{I = 1/2\} = 0.437 m_\pi^{-1} \quad a_{\pi \Delta}\{I = 3/2\} = 0.175 m_\pi^{-1} \quad a_{\pi \Delta}\{I = 5/2\} = -0.262 m_\pi^{-1} \quad (8.2)$$

#### Acknowledgments

The work of G. Marques is supported by Fundação para a Ciência e a Tecnologia under the grant SFRH/BD/984/2000.

Quark and Antiquark propagators

$S(\mathbf{k}, w, \mathbf{k}', w')$	$(2\pi)^4 \delta^3(\mathbf{k} - \mathbf{k}') \delta(w - w') (-i) / (w - E(\mathbf{k}) + i\epsilon)$
Quark vertex $\Gamma^{++}$	$u_s^\dagger(k) \beta \Gamma u_{s'}(k')$
Antiquark vertex $\Gamma^{--}$	$v_s^\dagger(k) \beta \Gamma v_{s'}(k')$
Creation vertex $\Gamma^{+-}$	$u_s^\dagger(k) \beta \Gamma v_{s'}(k')$
Annihilation vertex $\Gamma^{-+}$	$v_s^\dagger(k) \beta \Gamma u_{s'}(k')$
Vertices $\Gamma = \beta$	
$u_s^\dagger(\mathbf{k}_1) u_{s'}(\mathbf{k}_2)$	$\frac{1}{2} [(\sqrt{1 + S_1} \sqrt{1 + S_2} + \sqrt{1 - S_1} \sqrt{1 - S_2}) \delta_{ss'} +$ $+ \sqrt{1 - S_1} \sqrt{1 - S_2} (i\sigma \cdot \hat{\mathbf{k}}_1 \times \hat{\mathbf{k}}_2)_{ss'}]$
$-v_s^\dagger(\mathbf{k}_1) v_{s'}(\mathbf{k}_2)$	$-\frac{1}{2} [(\sqrt{1 + S_1} \sqrt{1 + S_2} + \sqrt{1 - S_1} \sqrt{1 - S_2}) \delta_{ss'} +$ $+ \sqrt{1 - S_1} \sqrt{1 - S_2} (i\sigma \cdot \hat{\mathbf{k}}_1 \times \hat{\mathbf{k}}_2)_{ss'}^*]$
$v_s^\dagger(\mathbf{k}_1) u_{s'}(\mathbf{k}_2)$	$\frac{1}{2} [\sqrt{1 - S_1} \sqrt{1 + S_2} \hat{\mathbf{k}}_1 - \sqrt{1 + S_1} \sqrt{1 - S_2} \hat{\mathbf{k}}_2] \cdot (\sigma i \sigma_2)_{ss'}$
$v_s^\dagger(\mathbf{k}_1) u_{s'}(\mathbf{k}_2)$	$-\frac{1}{2} [\sqrt{1 - S_1} \sqrt{1 + S_2} \hat{\mathbf{k}}_1 - \sqrt{1 + S_1} \sqrt{1 - S_2} \hat{\mathbf{k}}_2] (\sigma i \sigma_2)_{ss'}^*$
Vertices $\Gamma = \gamma$	
$u_s^\dagger(\mathbf{k}_1) \alpha u_{s'}(\mathbf{k}_2)$	$\frac{1}{2} \left( \sqrt{1 - S_1} \sqrt{1 + S_2} \hat{\mathbf{k}}_1 + \sqrt{1 + S_1} \sqrt{1 - S_2} \hat{\mathbf{k}}_2 \right) \delta_{ss'} +$ $+ \frac{1}{2} \left( -\sqrt{1 - S_1} \sqrt{1 + S_2} \hat{\mathbf{k}}_1 + \sqrt{1 + S_1} \sqrt{1 - S_2} \hat{\mathbf{k}}_2 \right) \times \sigma_{ss'}$
$u_s^\dagger(\mathbf{k}_1) \alpha v_{s'}(\mathbf{k}_2)$	$\frac{1}{2} \sqrt{1 + S_1} \sqrt{1 + S_2} [\sigma (i \sigma_2)]_{ss'} -$ $- \frac{1}{2} \sqrt{1 - S_1} \sqrt{1 - S_2} [\hat{\mathbf{k}}_1 \cdot \sigma \hat{\mathbf{k}}_2 + \hat{\mathbf{k}}_2 \cdot \sigma \hat{\mathbf{k}}_1 - \hat{\mathbf{k}}_1 \cdot \hat{\mathbf{k}}_2 \sigma - i \hat{\mathbf{k}}_1 \times \hat{\mathbf{k}}_2] (i \sigma_2)_{ss'}$
meson propagator $\underline{\underline{}}$	$i/(P^0 - E(\mathbf{P}) + i\epsilon)$
meson wave function ( $P_0 > 0$ ) $\phi^+$	$\frac{1}{\sqrt{2E}} u_s^\dagger(k) \beta \chi v_{s'}(k') / (P_0 - E(\mathbf{k}) - E(\mathbf{k}') + i\epsilon)$
meson wave function ( $P_0 < 0$ ) $\phi^-$	$\frac{1}{\sqrt{2E}} v_s^\dagger(k) \beta \chi u_{s'}(k') / (P_0 - E(\mathbf{k}) - E(\mathbf{k}') + i\epsilon)$
quark meson vertex $Z$	$u_s^\dagger(k) \beta \chi u_{s'}(k') / \sqrt{2E}$
antiquark meson vertex $Z$	$v_s^\dagger(k) \beta \chi v_{s'}(k') / \sqrt{2E}$

TABLE III: A set of Feynman rules.  $S_1 = \sin(\varphi(k1))$ ;  $S_2 = \sin(\varphi(k2))$ ;  $\chi$  is the mesonic Bethe-Salpeter vertex

## APPENDIX A: FEYNMAN RULES

In section VI we resort to the usual set of Feynman rules where the quark vertices are just  $\Gamma$ , with the spinors contained in the Feynman propagator.

$$\langle 0 | T[\psi_\alpha(x_1) \bar{\psi}_\beta(x_2)] | 0 \rangle = \int \frac{d^4 p}{(2\pi)^4} e^{-ip(x_1 - x_2)} \left( \frac{\Lambda_{\alpha\beta}^+(\mathbf{p}) \beta}{p_0 - E(\mathbf{p}) + i\epsilon} + \frac{\beta \Lambda_{\alpha\beta}^-(\mathbf{p})}{p_0 + E(\mathbf{p}) - i\epsilon} \right) \quad (\text{A1})$$

where  $\Lambda_{\alpha\beta}^+$  is given by  $\sum_s u_\alpha(s, \mathbf{p}) u_\beta^\dagger(s, \mathbf{p})$  and  $\Lambda_{\alpha\beta}^-$  by  $\sum_s v_\alpha(s, \mathbf{p}) v_\beta^\dagger(s, \mathbf{p})$ . Using the spinor definitions,

$$u_s(\mathbf{p}) = \left[ \sqrt{\frac{1 + \sin \varphi}{2}} + \sqrt{\frac{1 - \sin \varphi}{2}} \hat{\mathbf{p}} \cdot \boldsymbol{\alpha} \right] u_s(\mathbf{0}); \quad v_s(\mathbf{p}) = \left[ \sqrt{\frac{1 + \sin \varphi}{2}} - \sqrt{\frac{1 - \sin \varphi}{2}} \hat{\mathbf{p}} \cdot \boldsymbol{\alpha} \right] v_s(\mathbf{0}). \quad (\text{A2})$$

we obtain for  $\Lambda^\pm$ ,

$$\Lambda^\pm(\mathbf{k}) = (1 \pm \sin(\varphi(\mathbf{k})) \beta \pm \cos(\varphi(\mathbf{k}))) \boldsymbol{\alpha} \cdot \hat{\mathbf{k}} / 2. \quad (\text{A3})$$

In Table A we summarize the two equivalent set of Feynman rules used throughout this paper and give the dictionary between them. A covariant meson propagator going like  $(P^2 - M^2)^{-1}$  can be used instead of  $(P^0 - E(\mathbf{P}) + i\epsilon)^{-1}$  provided we divide our meson Salpeter amplitudes by  $\sqrt{2E(\mathbf{P})}$ . Then, for any  $T$  matrix, involving  $n$  mesons, we correct for this factor  $(\sqrt{2E(\mathbf{P})})^{-n}$  by a multiplicative factor  $(\sqrt{2E(\mathbf{P})})^n$ . Because  $E(\mathbf{0}) = m_\pi$ , we have the factor  $(\sqrt{2m_\pi})^4$  appearing in Eq.(5.4). Next we apply these Feynman rules to obtain some of the basic results widely used in the paper.

## APPENDIX B: FLAVOR TRACES AND CALCULATIONS

### 1. $\pi\pi$ traces

In what concerns flavor, we have two different cases,  $I = 0$  and  $I = 2$ . The  $I = 1$  is antisymmetric it would contribute to the p-wave scattering, but it does not affect the scattering length. The flavor contributions to the pion vertex factorize from the momentum contribution. The flavor kets, which correspond to the pair of incoming pions, are computed with the usual SU(2) flavor wave functions for the pion and with the usual Clebsh Gordan coefficients. A convenient notation is obtained with the use of Pauli matrices. The flavor kets are respectively

$$\begin{aligned} |00\rangle &= \frac{|\pi^0\pi^0 - \pi^+\pi^- - \pi^-\pi^+|}{\sqrt{3}} = \frac{|(u\bar{u} - d\bar{d})^2/2 + u\bar{d}d\bar{u} + d\bar{u}u\bar{d}|}{\sqrt{3}} = \frac{\tau_{f,f'} \cdot \tau_{f'',f'''}}{2\sqrt{3}} \\ |22\rangle &= |\pi^+\pi^+| = |u\bar{d}u\bar{d}| = \tau_{f,f'}^+ \tau_{f'',f'''}^+ . \end{aligned} \quad (B1)$$

The flavor bras are the Hermitian conjugate of these kets, they correspond to the outgoing pions, and we get,

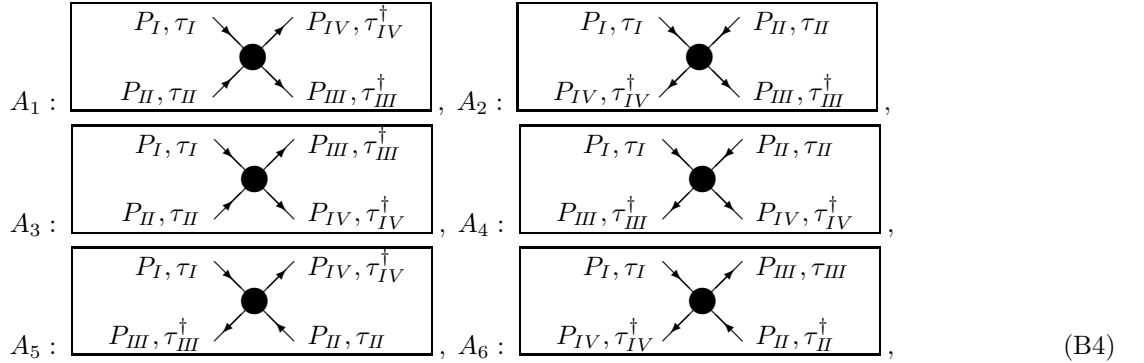
$$\langle 00| = \frac{\tau_{f,f'} \cdot \tau_{f'',f'''}}{2\sqrt{3}}, \quad \langle 22| = \tau_{f,f'}^- \tau_{f'',f'''}^- , \quad (B2)$$

where  $f, f', f'', f'''$  are the flavor indices of the quarks.

The different Feynman loops which contribute to the  $T$  matrix produce two classes of flavor results. The incoming and outgoing pion pairs are either directly connected to the loop, or cross before they connect to the loop. The flavor loops are,

direct:	crossed:
$I = 0 : \frac{1}{12} \text{Tr}\{(\boldsymbol{\tau} \cdot \boldsymbol{\tau})(\boldsymbol{\tau} \cdot \boldsymbol{\tau})\} = \frac{3}{2}$	$\frac{1}{12} \sum_{ij} \text{Tr}\{\tau_i \tau_j \tau_i \tau_j\} = -\frac{1}{2}$
$I = 2 : \text{Tr}\{(\tau^+ \tau^+)(\tau^- \tau^-)\} = 0$	$\text{Tr}\{\tau^+ \tau^- \tau^+ \tau^-\} = 1$

There are six different possible diagrams. We display them in the next figure, with the convention that the flavor and momentum of the two incoming pions are,  $P_I, \tau_I$ ,  $P_{II}, \tau_{II}$  and that the flavor and momentum of the two outgoing pions are,  $-P_{III}, \tau_{III}^\dagger$ ,  $-P_{IV}, \tau_{IV}^\dagger$ . The direct diagrams are the first 4 ones,  $A_1, A_2, A_3, A_4$  and the crossed diagrams are the last two,  $A_5, A_6$ ,



where  $A_2, A_4, A_6$  are respectively identical to  $A_1, A_3, A_5$  except that they have a reversed direction of the fermion propagators in the loop. Nevertheless they produce the same result,  $A_2 = A_1$ ,  $A_4 = A_3$ ,  $A_6 = A_5$ . We also have  $A_3 = \mathcal{P}_{III,IV} A_1$ ,  $A_5 = \mathcal{P}_{II,III} A_1$ , meaning for instance, that diagram  $A_3$  can be obtained from diagram  $A_1$  by interchanging the outgoing pion  $III$  and  $IV$ .

### 2. $\pi N$ traces

For  $\pi - N$  we have the cases of isospin  $3/2$  and  $1/2$ .

$$\begin{aligned} (I = 3/2) : p\pi^+, \frac{1}{\sqrt{3}}(n\pi^+ + \sqrt{2}p\pi^0), \frac{1}{\sqrt{3}}(\sqrt{2}n\pi^0 + p\pi^-), n\pi^- \\ (I = 1/2) : \frac{1}{\sqrt{3}}(\sqrt{2}n\pi^+ - p\pi^0), \frac{1}{\sqrt{3}}(n\pi^0 - \sqrt{2}p\pi^-) \end{aligned} \quad (B5)$$

$\mathcal{E}$	$V_{N3}$	$V_{E1}$	$V_{E2}$	$V_{A1}$
$\frac{1}{3}$	$-\frac{2}{9}$	$\frac{4}{9}$	$-\frac{2}{9}$	$\frac{4}{9}$

TABLE IV: Color contributions.

	$N\pi$	$\Delta\pi$
	F	D
$\mathcal{E}$	$\frac{1}{2}I$	$\frac{1}{2}I + \frac{2}{3}\tau_N \cdot \tau_\pi$
$V_{E1}$	$\frac{1}{2}I$	$\frac{1}{2}I + \frac{2}{3}\tau_N \cdot \tau_\pi$
$V_{E2}$	$\frac{1}{2}I$	$\frac{1}{2}I + \frac{2}{3}\tau_N \cdot \tau_\pi$
$V_{N3}$	$\frac{1}{2}I + \tau_N \cdot \tau_\pi$	$\frac{1}{2}I - \frac{1}{3}\tau_N \cdot \tau_\pi$
$V_{A1}$	$\frac{1}{2}I$	$\frac{1}{2}I - \frac{2}{3}\tau_N \cdot \tau_\pi$

TABLE V: Flavor contributions.  $\tau_N$ ,  $\tau_\pi$  and  $\tau_\Delta$  are, respectively, the isospin generators acting in  $I=1/2$ , 1 and  $3/2$  isospin wave functions. The  $I$  represents the identity operator in flavor space

The isospin contribution of any diagram must be a linear combination of the Identity and  $\tau_N \cdot \tau_\pi$ , where

$$\tau_N \cdot \tau_\pi = \frac{1}{2}((\tau_\pi + \tau_N)^2 - \tau_\pi^2 - \tau_N^2) = \frac{1}{2}(I(I+1) - 2 - \frac{3}{4}). \quad (B6)$$

The computation of these contributions was done exhaustively for each diagram and each multiplet element. The results are presented in Table IV.

In the same way for  $\Delta - \pi$  we have isospin  $5/2$ ,  $3/2$  and  $1/2$ .

$$\begin{aligned}
 & (I=5/2) : \\
 & \Delta^{++}\pi^+, \frac{1}{\sqrt{5}}(\sqrt{2}\Delta^{++}\pi^0 + \sqrt{3}\Delta^+\pi^+), \frac{1}{\sqrt{10}}(\Delta^{++}\pi^- + \sqrt{6}\Delta^+\pi^0 + \sqrt{3}\Delta^0\pi^+) \\
 & \frac{1}{\sqrt{10}}(\sqrt{3}\Delta^+\pi^- + \sqrt{6}\Delta^0\pi^0 + \Delta^-\pi^+), \frac{1}{\sqrt{5}}(\sqrt{3}\Delta^0\pi^- + \sqrt{2}\Delta^-\pi^0), \Delta^-\pi^- \\
 & (I=3/2) : \\
 & \frac{1}{\sqrt{5}}(\sqrt{3}\Delta^{++}\pi^0 - \sqrt{2}\Delta^+\pi^+), \frac{1}{\sqrt{15}}(\sqrt{2}\Delta^{++}\pi^- + \Delta^+\pi^0 - \sqrt{8}\Delta^0\pi^+), \\
 & \frac{1}{\sqrt{15}}(\sqrt{8}\Delta^+\pi^- - \Delta^0\pi^0 - \sqrt{2}\Delta^-\pi^+), \frac{1}{\sqrt{5}}(\sqrt{2}\Delta^0\pi^- - \sqrt{3}\Delta^-\pi^0) \\
 & (I=1/2) : \\
 & \frac{1}{\sqrt{6}}(\sqrt{3}\Delta^{++}\pi^- - \sqrt{2}\Delta^+\pi^0 + \Delta^0\pi^+), \frac{1}{\sqrt{6}}(\Delta^+\pi^- - \sqrt{2}\Delta^0\pi^0 + \sqrt{3}\Delta^-\pi^+)
 \end{aligned} \quad (B7)$$

In this case the isospin contributions must be a linear combination of the Identity,  $\tau_\Delta \cdot \tau_\pi$  and  $(\tau_\Delta \cdot \tau_\pi)^2$ , once more where

$$\tau_\Delta \cdot \tau_\pi = \frac{1}{2}((\tau_\pi + \tau_\Delta)^2 - \tau_\pi^2 - \tau_\Delta^2) = \frac{1}{2}(I(I+1) - 2 - \frac{15}{4}). \quad (B8)$$

Table IV includes also the isospin structures of each diagram in this case.

The spin structures of  $\pi$ ,  $N$  and  $\Delta$  wave functions, together with the spin vector structure  $\rho$ , later needed in the calculations, can be written as,

$$\begin{aligned}
 \Sigma^\pi &= (i\sigma_2/\sqrt{2})_{ab}; \quad \Sigma_s^\rho = [\boldsymbol{\sigma}i\sigma_2/\sqrt{2}]_{ab} \cdot \mathbf{v}_s; \quad \Sigma_s^\Delta = [\boldsymbol{\sigma}i\sigma_2/\sqrt{2}]_{ab} \cdot \mathbf{w}_{cs}; \\
 \Sigma_s^{N^F} &= (i\sigma_2/\sqrt{2})_{ab} \delta_{cs}; \quad \Sigma_s^{N^D} = (1/\sqrt{3}) [\boldsymbol{\sigma}i\sigma_2/\sqrt{2}]_{ab} \cdot \boldsymbol{\sigma}_{cs}
 \end{aligned} \quad (B9)$$

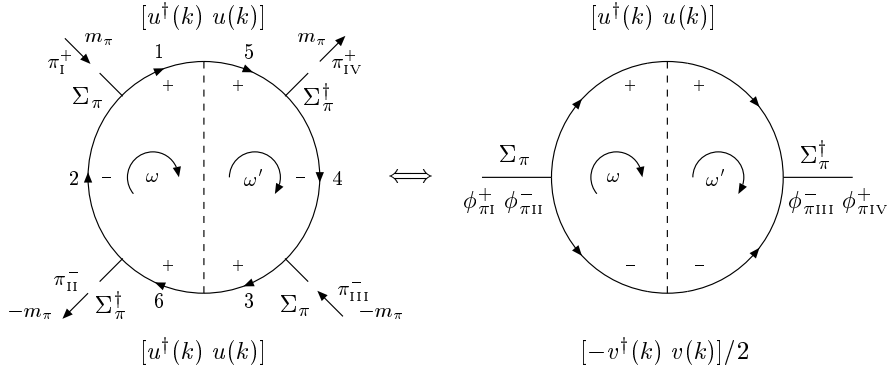


FIG. 17: An example of the map  $\pi \otimes \pi \rightarrow \pi$  contributing to  $V^{++}$ . We changed the arrow sense in the lower part of the leftmost fermion loop to be consistent with the Goldstone diagrammatic rules of Table A. Notice that the Wick minus sign from the fermion loop (or if we want from the quark exchange-see Fig. 6) gets transferred to the minus sign multiplying  $v^\dagger(k) v(k)$

where  $a$ ,  $b$  and  $c$  stand for the quarks individual spin, whereas  $s$  stands for the **total** spin of the meson or baryon under consideration. For example, we have,

$$\begin{bmatrix} \uparrow & \downarrow \end{bmatrix} \Sigma^\pi \begin{bmatrix} \uparrow \\ \downarrow \end{bmatrix} = \frac{1}{\sqrt{2}} (\uparrow\downarrow - \downarrow\uparrow).$$

The vectors  $\mathbf{v}_s$  and  $\mathbf{w}_{cs}$ , are given by,

$$\begin{aligned} \mathbf{v}_1 &= (1/\sqrt{2}, -i/\sqrt{2}, 0), \quad \mathbf{v}_0 = (0, 0, -1), \quad \mathbf{v}_{-1} = (1/\sqrt{2}, i/\sqrt{2}, 0), \\ \mathbf{w}_{c\frac{3}{2}} &= \mathbf{v}_1 \delta_{c\frac{1}{2}}, \quad \mathbf{w}_{c\frac{1}{2}} = 1/\sqrt{3} \mathbf{v}_1 \sigma_{c\frac{1}{2}}^+ + \sqrt{2/3} \mathbf{v}_0 \delta_{c\frac{1}{2}}, \\ \mathbf{w}_{c-\frac{1}{2}} &= 1/\sqrt{3} \mathbf{v}_{-1} \sigma_{c-\frac{1}{2}}^- + \sqrt{2/3} \mathbf{v}_0 \delta_{c-\frac{1}{2}}, \quad \mathbf{w}_{c-\frac{3}{2}} = \mathbf{v}_{-1} \delta_{c-\frac{1}{2}}. \end{aligned} \quad (B10)$$

They have the properties,

$$v_s^{i\dagger} v_{s'}^j = \delta_{ss'} \delta^{ij} - (J^i J^j)_{ss'}, \quad w_{sc}^i w_{cs'}^j = \delta_{ss'}. \quad (B11)$$

where the  $J$ 's are the spin 1 SU(2) generating matrices. The importance of the above spin functions lies in the fact that they map the quark spin content of a given bound state to the total spin of that bound state. Once this map is achieved, then it is a matter of straightforward calculations to obtain the diagrammatic traces.

### APPENDIX C: THE MAPPING $\pi \otimes \pi \rightarrow \pi$

In this section we show that we can map the scattering amplitude  $\pi\pi \rightarrow \pi\pi$  into the Salpeter equation for one pion, the only difference being that we will have instead of the usual single pion Salpeter momentum-space wave functions  $\phi^\alpha(k)$ , specific products of two such functions  $\phi^\beta(k) \phi^\gamma(k)$ , with  $\alpha, \beta, \gamma = \pm$ . These mappings can be done for all possible  $\pi^\pm \pi^\pm \pi^\pm \pi^\pm$  diagrams, consistent with energy conservation. It is not hard to see that the requirement of energy conservation implies that only diagrams with none or an even number of  $\pi^-$  may exist. Finally the pluses and minuses (meaning the Feynman projectors  $\Lambda^\pm$ ) appearing in the quark loop connecting the four pion sources are subjected to the constraint that the signs immediately adjacent to any such pion source, should be different. In this way we are able to draw all possible diagrams contributing to  $\pi\pi$  scattering. To illustrate the mapping  $\pi \otimes \pi \rightarrow \pi$  we consider two examples. All the other diagrams can be mapped the same way. The first example is depicted in figure 17 for the flavor traces  $b_{[0,2]} = [3/2, 0]$ ,

Using Eqs.(4.2), (4.4) and

$$\Sigma_\pi (u^\dagger(k) u(k)) \Sigma_\pi = \frac{1}{2} (-v^\dagger(k) v(k)) \quad (C1)$$

to bring  $u^\dagger(k) u(k)$  into  $-v^\dagger(k) v(k)$  it is not hard to see that this diagram contributes as,

$$[\phi_{\pi I}^+ \phi_{\pi II}^-, \times] \begin{bmatrix} V^{++} & \times \\ \times & \times \end{bmatrix} \begin{bmatrix} \phi_{\pi III}^+ \phi_{\pi IV}^- \\ \times \end{bmatrix} \quad (C2)$$

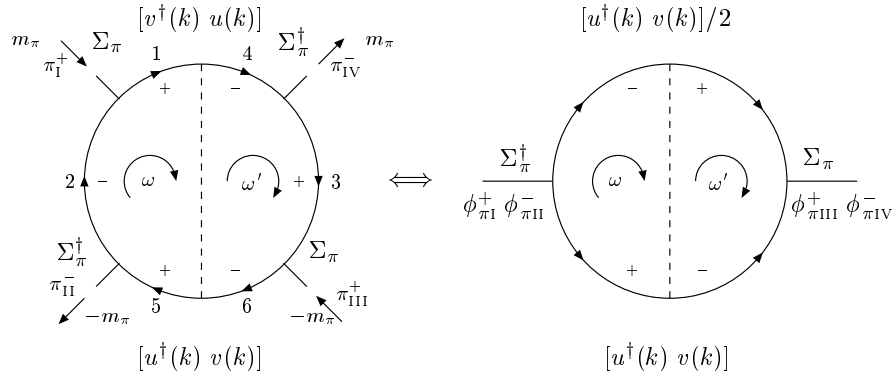


FIG. 18: An example of the map  $\pi \otimes \pi \rightarrow \pi$  contributing to  $V^{-+}$

The second example, again for  $b_{[0,2]} = [3/2, 0]$ , is depicted in figure 18. In this figure we use the equation

$$\Sigma_\pi(v^\dagger(k)u(k))\Sigma_\pi^\dagger = \frac{1}{2}(v^\dagger(k)u(k)) \quad (C3)$$

to obtain,

$$[\phi_{\pi I}^+ \phi_{\pi II}^-, \times] \begin{bmatrix} \times & V^{+-} \\ \times & \times \end{bmatrix} \begin{bmatrix} \times \\ \phi_{\pi III}^+ \phi_{\pi IV}^- \end{bmatrix} \quad (C4)$$

In fact, in the case of the diagrams with a kernel insertion, for every contribution (like those of Eqs. (17-C2, 18-C4)) we can always find another diagram which yields the same value, so that we need only to consider half of the diagrams and multiply the result by two. Because we have in Eq.(5.1) four kinetic insertions  $T_i$ , which are identical in the case of zero incoming momenta, and noticing that the corresponding number of (identical) kinetic operators for the mesonic Salpeter equation (for mesons at rest) is two, we have that this degeneracy is just what we need to bring us an overall factor of two:  $2(T + T + V^{\pm\pm}) = 2H_{one\ meson}^{\pm\pm}$ . So in Eq.(5.1), the kinetic terms  $T_i$  are added to the  $V^{++}$  and  $V^{--}$  terms like those of Eqs. (C2, C4) to obtain similar equations now having  $H^{++}, H^{--}$  instead of  $V^{++}, V^{--}$ . The number of normalization diagrams is exactly what it is needed to bring all  $V^{++}, V^{--}, V^{+-}, V^{-+}$  equations to the  $H^{++}, H^{--}, H^{+-}, H^{-+}$  type.

The term,

$$[\phi^{+2}, \phi^{-2}] \sigma_3 m_\pi \begin{bmatrix} \phi^{+2} \\ \phi^{-2} \end{bmatrix} \quad (C5)$$

present in Eq.(5.4) also comes from the normalization diagrams. An example of one such diagram is given in Fig. 6. Upon integration in the energies flowing in the quark loop we always get Eq.(5.1) where  $\sum p_i^0$  equals  $[\pm m_\pi]_I + [\pm m_\pi]_{II}$ , depending on the particular case of  $\pi_I^\pm \pi_{II}^\pm$  under consideration or, because total energy is conserved,  $\sum p_i^0 = [\pm m_\pi]_{III} + [\pm m_\pi]_{IV}$ , on the corresponding outgoing configuration  $\pi_{III}^\pm \pi_{IV}^\pm$ . Notice that total energy conservation enforces, for a particular energy-spin configuration of the incoming pions, a consistent energy-spin configuration of the outgoing pions. For instance if we have  $\pi^+ \pi^-$  for incoming states we must have exactly one  $\pi^-$  among the outgoing states. Only incoming (or outgoing) terms like  $\phi^{+2}$  or terms like  $\phi^{-2}$  will have non-vanishing values for  $\sum p_i^0$ . They are  $+2m_\pi, -2m_\pi$  respectively. Again we have the same factor of two as before. This will bring in the matrix  $2m_\pi \sigma_3$ . In this way we are able to obtain Eq.(5.4). Finally in color space it is straight forward to see that the mapping  $\pi \times \pi \rightarrow \pi$  will bring in a factor of  $1/3$  due to color normalization of the pion.

- [1] S. Weinberg, Phys. Rev. Lett. **17**, 616 (1966).
- [2] A. Chodos, R.L. Jaffe, K. Johnson, C.B. Thorn, and V.F. Weisskopf, Phys. Rev. D **9**, 3471 (1974); A. Chodos, R.L. Jaffe, K. Johnson, and C.B. Thorn, *ibid* **10**, 2599 (1974); T.A. de Grand, R.L. Jaffe, K. Johnson, and J. Kiskis, *ibid* **12**, 2060 (1975).
- [3] A. Chodos and C.B. Thorn, Phys. Rev. D. **12**, 2733 (1975); T. Inoue and T. Maskawa, Prog. Theor. Phys. **54**, 1833 (1975).

- [4] V. Vento, M. Rho and G.E. Brown, Nucl. Phys. **A345**, 413 (1980).
- [5] S. Théberge, A.W. Thomas, and G.A. Miller, Phys. Rev. D **22**, 2838 (1980); **23**, 2106(E) (1981); A.W. Thomas, S. Théberge, and G.A. Miller, *ibid* **24**, 216 (1981).
- [6] H.G. Dosch *Phys Lett.B* **190**, 177 (1987); H.G. Dosch and Yu A. Simonov *Phys Lett.B* **205**, 339 (1988).
- [7] A. Le Yaouanc, L. Oliver, O. Péne, and J.-C. Raynal, Phys. Rev. D **29**, 1233 (1984).
- [8] A. Le Yaouanc, L. Oliver, O. Péne, and J.-C. Raynal, Phys. Rev. D **31**, 137 (1985).
- [9] P. Bicudo and J. Ribeiro *Phys. Rev.D* **42**, 1611 (1990).
- [10] P. Bicudo and J. Ribeiro, Phys. Rev. D **42**, 1625 (1990); **42**, 1635 (1990).
- [11] P. Maris and P. Tandy, *Phys. Rev. C* **62** (2000); P. Maris, *Nucl. Phys. A* **663**, 621 (2000); P. Maris, e-Print Archive: nucl-th/0009064, to be published *Invited Talk in Proceedings of IV International Conference on Quark Confinement and the Hadron Spectrum, Vienna, Austria, 2000* (World Scientific, Singapore).
- [12] P. Bicudo, S. Cotanch, F. Llanes-Estrada, P. Maris, J. E. Ribeiro, A. Szczepaniak, *Phys. Rev. D* **65**:076008 (2002)
- [13] F. Llanes-Estrada and S. Cotanch, *Phys. Rev. Lett.* **84**, 1102 (2000).
- [14] P. Bicudo, J. E. Ribeiro, A. Nefediev, *Phys. Rev. D* **65** :085026 (2002)
- [15] J. Dias de Deus and J. Ribeiro *Phys. Rev. D* **21**, 1251 (1980).
- [16] J. Ribeiro, *Nuc. Phys. A* **689**, 247c (2001).
- [17] J. Ribeiro *Z. fur Phys. C* **5**, 27 (1980).
- [18] J. E. Ribeiro, *Phys. Rev. D* **25**, 2406 (1982); E. van Beveren, *Z. Phys. C* **17**, 135 (1982).